Delay in Feedback Repression by *Cryptochrome 1* Is Required for Circadian Clock Function

Maki Ukai-Tadenuma,[1,8] Rikuhiro G. Yamada,[1,8] Haiyan Xu,[4] Jürgen A. Ripperger,[5] Andrew C. Liu,[4] and Hiroki R. Ueda[1,2,3,6,7,*]

[1]Laboratory for Systems Biology, RIKEN Center for Developmental Biology
[2]Functional Genomics Unit, RIKEN Center for Developmental Biology
[3]Laboratory for Synthetic Biology, RIKEN Quantitative Biology Center
2-2-3 Minatojima-minamimachi, Chuo-ku, Kobe, Hyogo 650-0047, Japan
[4]Department of Biological Sciences, The University of Memphis, Memphis, TN 38152-0001, USA
[5]Department of Medicine/Unit of Biochemistry, University of Fribourg, 5, rue du Musée, CH-1700 Fribourg, Switzerland
[6]Graduate School of Science, Osaka University, 1-1 Machikaneyama, Toyonaka, Osaka 560-0043, Japan
[7]Department of Mathematics, Graduate School of Science, Kyoto University, Kitashirakawa Oiwake-cho, Sakyo-ku, Kyoto, Kyoto 606-8502, Japan
[8]These authors contributed equally to this work
*Correspondence: uedah-tky@umin.ac.jp
DOI 10.1016/j.cell.2010.12.019

SUMMARY

Direct evidence for the requirement of delay in feedback repression in the mammalian circadian clock has been elusive. *Cryptochrome 1* (*Cry1*), an essential clock component, displays evening-time expression and serves as a strong repressor at morning-time elements (E box/E′ box). In this study, we reveal that a combination of day-time elements (D box) within the *Cry1*-proximal promoter and night-time elements (RREs) within its intronic enhancer gives rise to evening-time expression. A synthetic composite promoter produced evening-time expression, which was further recapitulated by a simple phase-vector model. Of note, coordination of day-time with night-time elements can modulate the extent of phase delay. A genetic complementation assay in *Cry1*$^{-/-}$:*Cry2*$^{-/-}$ cells revealed that substantial delay of *Cry1* expression is required to restore circadian rhythmicity, and its prolonged delay slows circadian oscillation. Taken together, our data suggest that phase delay in *Cry1* transcription is required for mammalian clock function.

INTRODUCTION

Circadian clocks are thought to consist of autoregulatory loops with delayed transcriptional/translational feedback repression in which delayed expression of clock components is critical for maintaining circadian rhythmicity (Dunlap, 1999; Reppert and Weaver, 2002; Young and Kay, 2001). However, the underlying molecular mechanism giving rise to such delay remains unknown, hindering formal validation of its biological relevance. In mammalian clocks, circadian transcriptional program is mediated through at least three clock-controlled DNA elements, morning-time (E box/E′ box, or E/E′ box: CACGT[G/T]) (Gekakis, 1998; Hogenesch et al., 1997; Ueda et al., 2005; Yoo et al., 2005), day-time (D box: TTA[T/C]GTAA) (Falvey et al., 1996; Ueda et al., 2005), and night-time elements (*Rev-Erb*/*ROR*-binding element, or RRE: [A/T]A[A/T]NT[A/G]GGTCA) (Harding and Lazar, 1993; Preitner et al., 2002; Ueda et al., 2002, 2005). The E/E′ box-mediated transcriptional program has a critical role in the core autoregulatory loop of the mammalian circadian clock (Gekakis, 1998; Sato et al., 2006; Ueda et al., 2005). In this core loop, bHLH-PAS transcription activators such as BMAL1 and CLOCK form heterodimers that bind to E/E′ box *cis*-elements in the promoter regions of their target genes, including the *Per* and *Cry* genes; CRYs, in turn, form repressor complexes that physically associate with the BMAL1/CLOCK complex to inhibit E/E′ box-mediated transcription (Dunlap, 1999; Griffin et al., 1999; Kume et al., 1999; Reppert and Weaver, 2002; Young and Kay, 2001). Thus, the CRYs play an integral role in the circadian clock by "closing" the core negative feedback loop.

Although *Cry1*$^{-/-}$ mice and their SCN slices display circadian rhythms at the organismal and tissue levels, respectively, dissociated *Cry1*$^{-/-}$ SCN neurons and fibroblasts are largely arrhythmic. The issue of cell autonomy has been carefully examined in several recent studies (Brown et al., 2005; DeBruyne et al., 2007; Liu et al., 2007). By contrast to *Cry1*-deficient cells, dissociated *Cry2*$^{-/-}$ SCN neurons and fibroblasts exhibit robust rhythmicity, implying that CRY2 cannot substitute for *Cry1* deficiency at the cellular level (Liu et al., 2007). Therefore, we focused on transcriptional regulation of *Cry1* gene.

CRY1 and its expression pattern play a pivotal role in the core autoregulatory loop. Either overexpression of CRY1 or interference of CRY1's repressor activity on E/E′ box-mediated

transcription can abolish circadian transcriptional oscillations (Sato et al., 2006; Ueda et al., 2005). Remarkably, *Cry1* displays delayed gene expression relative to other genes with E/E′ box elements (Ueda et al., 2002, 2005). Circadian expression of *Cry1* peaks at evening phases in the SCN (∼CT12) (Ueda et al., 2002, 2005), which is much later than for typical morning-time E/E′ box-regulated genes such as *Rev-Erbα*, and is intermediate between day-time D box- and night-time RRE-regulated genes such as *Per3* and *Bmal1*, respectively (Ueda et al., 2002, 2005). Dual roles of *Cry1* as a strong repressor for E/E′ box activity and a time delay mediator fit well with the current model of the circadian clock, i.e., feedback repression with delay may depend on the unique mode of transcriptional regulation of *Cry1*.

Previous studies identified an E′ box and an E box in *Cry1*'s regulatory region (Ueda et al., 2005; Fustin et al., 2009) and two RREs in its first intron (Ueda et al., 2005). In this study, we also identified additional D boxes in the promoter region and confirmed their functionality in conferring day-time expression (delayed phase relative to E box). We further discovered that a combination of the promoter containing E/E′ boxes and D boxes with the first intron sequence of *Cry1* containing RREs generated delayed-phase expression of *Cry1*, in which the strength of night-time elements (RREs) can modulate the extent of phase delay. Of note, a simple phase vector model predicts that coordination between day-time and night-time elements can determine the extent of phase delay. Based on this model, we generated an array of *Cry1* constructs that display different phases, and these constructs were used in a genetic complementation assay to restore circadian oscillation in *Cry1*$^{-/-}$:*Cry2*$^{-/-}$ cells. These experiments reveal that substantial delay of *Cry1* expression is required to restore single-cell level rhythmicity and that prolonged delay of *Cry1* expression can slow circadian oscillation. These results suggest that phase delay in transcriptional feedback repression is required for mammalian clock function.

RESULTS

Cry1 Promoter Confers Phase and Amplitude Intermediate between Those Conferred by E/E′ Box and D Box Circadian Elements

To examine *Cry1* promoter activity, we generated a reporter construct, P(*Cry1*)-*Luc*, in which a 1.5 kbp DNA fragment containing the *Cry1* promoter was fused to the *Luciferase* (*Luc*) gene. *Cry1* promoter-driven bioluminescence reached its peak at circadian time (CT) 9.60 ± 0.11 (n = 3, mean ± standard deviation), which was rather close to that of a D box-P(SV40)-*Luc* reporter harboring three tandem repeats of D boxes fused to an SV40 promoter (CT10.42 ± 0.16), and delayed > 6 hr relative to an E′ box-P(SV40)-*Luc* reporter harboring three tandem repeats of E′ boxes fused to an SV40 promoter (CT3.53 ± 0.04) (Figure 1A and Figure S1A and Table S1 available online). On the other hand, the *Cry1* promoter produced a higher-amplitude rhythm than that of the D box-P(SV40)-*Luc* reporter (Figure 1B). The amplitude of E′ box-driven bioluminescence rhythms (Figure 1B, E′ box-P(SV40)-*Luc*) was even higher than those driven by the *Cry1* promoter. These data place the *Cry1* promoter intermediate between D box and E′ box in both phase and amplitude

of driven rhythms and suggest that the *Cry1* promoter might contain both D box and E′ box elements.

D Box in *Cry1* Promoter Confers Phase Delay and Day-Time Expression

We investigated the genomic sequences of the *Cry1* promoter and found five highly conserved regions, of which two sequences (5′-TTCAGAAA-3′ and 5′-AAACGTGA-3′) most closely resemble a D box according to position weight matrix analysis. Interestingly, these sequences overlap with the conserved E′ box sequences in the promoter region (Figure 1C). We designated this region of the *Cry1* promoter as a Cry1proD element and constructed a Cry1proD-P(SV40)-*Luc* reporter by fusing three tandem repeats of this element to an SV40 promoter. NIH 3T3 cells transiently transfected with this construct showed circadian oscillation of bioluminescence with a peak at day-time (CT12.37 ± 0.05, n = 3; Figure 1D, Figure S1B, and Table S1) and a relative amplitude between those of E′ box and D box constructs (Figure 1E). Because the E′ box and two putative D boxes in Cry1proD element overlap, it is not practical to isolate each CCE for analysis individually. Instead, we tested whether clock factors involved in E′ box- or D box-mediated transcription could activate or repress the Cry1proD element. Cotransfection of E′ box activators BMAL1/CLOCK strongly induced not only E′ box, but also Cry1proD activity in NIH 3T3 cells (Figure 1F). Cotransfection of a D box repressor E4BP4 inhibited BMAL1/CLOCK induction of Cry1proD activity in a dose-dependent manner (Figure 1F). Interestingly, the E′ box repressor CRY1 also inhibited this induction (Figure S1C), and the D box activators DBP, HLF, and TEF (Mitsui et al., 2001) also induced Cry1proD activity (Figure S1D). These results suggest that Cry1proD is regulated by classical transcriptional regulators of both D box and E/E′ box activities, consistent with the observation that bioluminescence rhythms driven by the *Cry1* promoter display properties intermediate between those driven by D box and E′ box constructs.

To confirm that *Cry1* expression is delayed relative to E/E′ box activity, we measured temporal mRNA profiles of endogenous *Per2*, *Bmal1*, and *Cry1* in NIH 3T3 cells expressing a P(*Cry1*)-*Luc* or a P(*Per2*)-*Luc* reporter (Figure 1G, left). As shown, the phase of *Luc* mRNA driven by the *Per2* promoter was almost the same as that of endogenous *Per2* mRNA (Figure 1G, right). Furthermore, the phase of *Luc* mRNA driven by the *Cry1* promoter was delayed relative to those of endogenous *Per2* mRNA or *Luc* mRNA driven by the *Per2* promoter, with a phase difference of ∼1–2 hr. These results further support the notion that functional D boxes in the *Cry1* promoter contribute to phase delay of *Cry1* expression.

Cry1 Intron Acts as an Enhancer to Confer Phase Delay

In addition to the phase delay caused by D boxes within the *Cry1* promoter, we also observed further phase delay of the endogenous *Cry1* mRNA by at least 2 hr relative to *Luc* mRNA driven by the *Cry1* promoter (Figure 1G). The endogenous *Cry1* mRNA displayed ∼3–4 hr phase delay relative to endogenous *Per2* mRNA and ∼7–8 hr advance relative to *Bmal1* mRNA. This observation is consistent with previous reports (Baggs et al., 2009; Etchegaray et al., 2003; Liu et al., 2008; Preitner
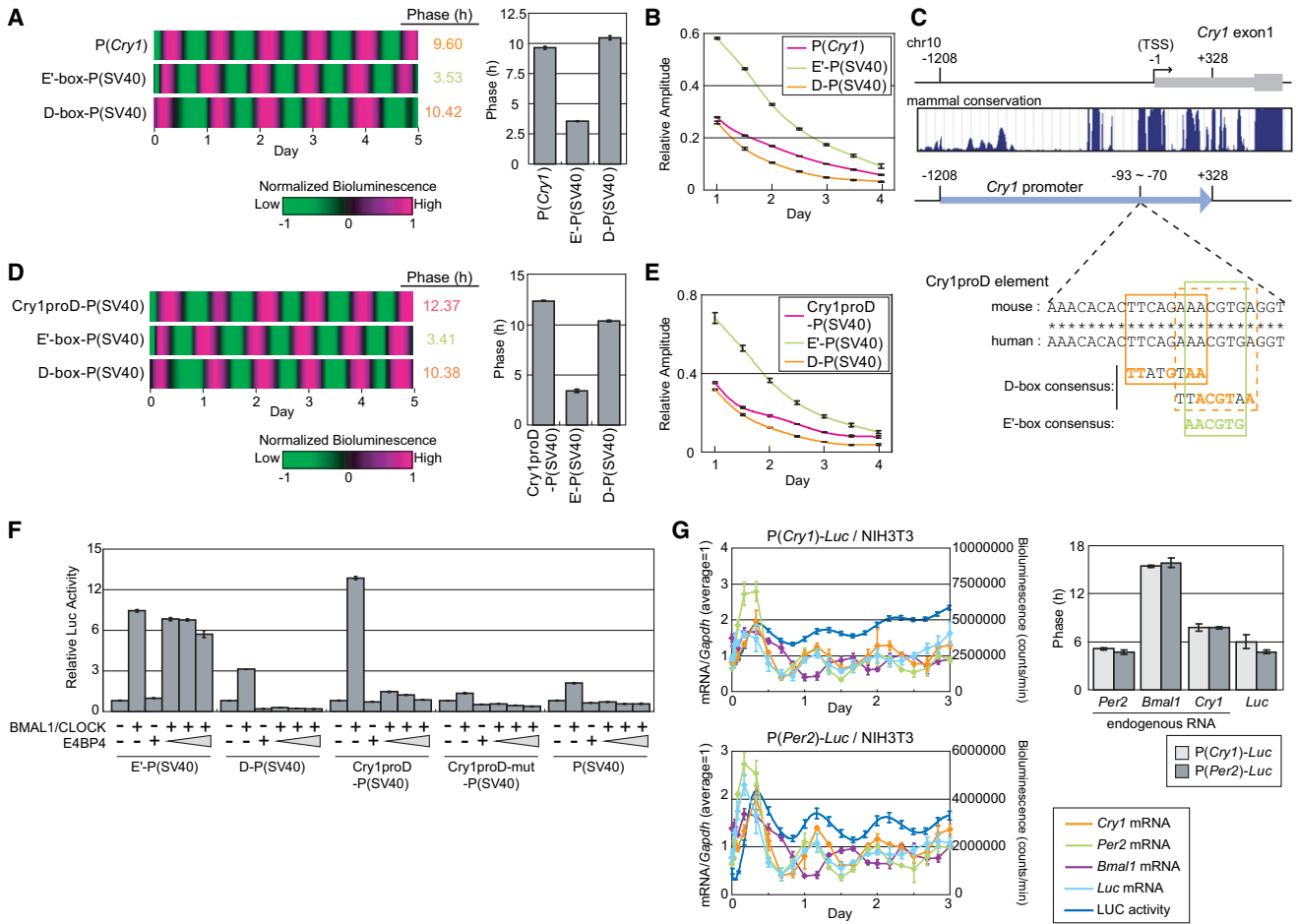
Figure 1. The *Cry1* Promoter Contains Both E/E′ Box and D Boxes

(A) The phases of circadian transcriptional activities induced by P(*Cry1*), E′ box-P(SV40), and D box-P(SV40) promoters. Each promoter was fused with a *Luciferase* reporter gene (*Luc*) and transiently transfected into NIH 3T3 cells. Time series of bioluminescence expression were recorded in real time using a photomultiplier tube (PMT). Heatmaps represent average promoter activities from three independent samples. Raw data were detrended for baseline and amplitude and then scaled into a range of −1 to 1 (left). Phases were estimated from the time series data by fitting a cosine wave (right).

(B) The relative amplitudes of circadian transcriptional activities induced by P(*Cry1*), E′ box-P(SV40), and D box-P(SV40) promoters.

(C) E′ box and its overlapping D boxes in *Cry1* promoter. Genomic positions relative to the transcription start site (TSS, designated also as "−1") of *Cry1* gene are indicated along with evolutionary conservation scores among mammalian species. Colored letters indicate nucleotides matching the consensus sequence of D box and E′ box.

(D) The phases of circadian transcriptional activities induced by Cry1proD-P(SV40), E′ box-P(SV40), and D box-P(SV40) promoters. The experiment was performed as in (A).

(E) The relative amplitudes of circadian transcriptional activities induced by Cry1proD-P(SV40), E′ box-P(SV40), and D box-P(SV40) promoters.

(F) The Cry1proD element can be activated by BMAL1/CLOCK and repressed by E4BP4. Each of the indicated promoters was fused to a *Luciferase* reporter gene and transiently transfected into NIH 3T3 cells. Relative *Luciferase* activity for each promoter was scaled so that the activity without transcriptional regulation is normalized to 1.

(A–F) Data are representative of two independent experiments. Error bars represent SD determined from three measurements for each sample (n = 3).

(G) mRNA expression patterns of endogenous *Cry1*, *Per2*, and *Bmal1* and exogenous *Luciferase* (*Luc*). NIH 3T3 cells were transfected with P(*Cry1*)-*Luc* or P(*Per2*)-*Luc* reporter. Relative mRNA levels of each gene were measured. In parallel, transcriptional activities of P(*Cry1*) and P(*Per2*) promoters were monitored by bioluminescence recording. Phases of measured rhythm are indicated on the right. (Right) Error bars represent SEM (n = 3). (Left) Error bars represent SD (n = 3). See also Figure S1 and Table S1.

et al., 2002; Sato et al., 2006; Ueda et al., 2005), which have speculated that a phase delay would be generated by two functional RREs present in the intron regions of *Cry1* (Ueda et al., 2005). To provide experimental evidence for the mechanism of further phase delay of *Cry1* expression, we focused on one of the highly conserved regions of the *Cry1* gene—the first intron, which contains two RREs, designated here as R1 and R2 (Figure 2A). These RREs are highly conserved and aligned in a head-to-head arrangement, perfectly matched to the consensus RRE sequence ([A/T]A[A/T]NT[A/G]GGTCA). We cloned a 1.03 kbp fragment containing the conserved intronic RREs and inserted it into the P(*Cry1*)-*Luc* reporter plasmid

to generate a P(*Cry1*)-*Cry1* intron 1.03k-*Luc* reporter. Cells expressing this reporter displayed a bioluminescence peak at CT14.62 ± 0.20, whereas absence of the 1.03 kbp intron sequence resulted in a peak at CT10.51 ± 0.30, a difference of ~4 hr (Figure 2B, Figure S2A, and Table S1). We next focused on a highly conserved region of 336 bp within the 1.03 kbp intron sequence for further analysis. Whereas cells expressing a P(*Cry1*)-*Cry1* intron Δ336-*Luc* reporter exhibited a peak at CT10.37 ± 0.24, those expressing P(*Cry1*)-*Cry1* intron 336-*Luc* peaked at CT14.32 ± 0.23 (Figure 2B, Figure S2A, and Table S1), a 4 hr phase delay. Thus, *Cry1* first intron sequences containing RREs likely underlie the delayed phase of *Cry1* expression. In addition, their effects appear to be independent of locations (Figure 2C, Figure S2B, and Table S1), suggesting that this sequence functions as a transcriptional enhancer.

Next, we analyzed the regulatory regions for the presence of their corresponding transcription factors in vivo using chromatin immunoprecipitation (ChIP) assays with time series samples from mouse liver. Chromatin from wild-type, $Dbp^{-/-}$ (Lopez-Molina et al., 1997), or $Rev\text{-}Erb\alpha^{-/-}$ (Preitner et al., 2002) mice was immunoprecipitated by anti-BMAL1, anti-DBP, or anti-REV-ERBα antibodies (Figure 2D). The levels of BMAL1 and DBP binding to Cry1proD displayed circadian oscillation in wild-type, $Dbp^{-/-}$, or $Rev\text{-}Erb\alpha^{-/-}$ mice, whereas DBP binding in $Dbp^{-/-}$ mice was significantly reduced (p < 0.01 by two-way ANOVA) with residual signals potentially deriving from TEF and/or HLF binding to the same element. On the other hand, no significant reduction was observed for the binding of DBP to this region in $Rev\text{-}Erb\alpha^{-/-}$ mice. The level of REV-ERBα binding to the *Cry1* first intron region also displayed circadian oscillation in wild-type and $Dbp^{-/-}$ mice, whereas it was significantly reduced in $Rev\text{-}Erb\alpha^{-/-}$ mice (p < 0.01 by two-way ANOVA). The levels of BMAL1 binding to the *Dbp* promoter region displayed circadian oscillation, whereas there was only background binding of DBP and REV-ERBα to this region. This result confirmed that BMAL1 and DBP bind to the *Cry1* promoter region, and REV-ERBα binds to the *Cry1* first intron region. The peak binding time of each transfactor is consistent with previous reports of its in vivo binding or its nuclear accumulation (Lopez-Molina et al., 1997; Mitsui et al., 2001; Preitner et al., 2002; Ripperger and Schibler, 2006).

In addition to the biochemical interaction between the *Cry1* promoter and D box *trans*-regulators described above, we also examined the role of the D box using genetic approaches; we measured mRNA expression patterns from time course liver samples of triple-knockout mice of PAR bZip genes (*Tef*, *Hlf*, and *Dbp*) (Gachon et al., 2004). Although these mice displayed normal circadian behavior (possibly due to compensation rendered by posttranslational mechanisms intracellularly and/or intercellular coupling of clock cells in vivo) (Gachon et al., 2004; Lee et al., 2001; Liu et al., 2007), we found that *Cry1*'s circadian expression level was different from wild-type and its peak of expression delayed (Figure 2E and Figure S2C), whereas those of other measured clock genes (*Bmal1*, *RevErbα*, and *Per1*) were not. Importantly, the observed peak delay was reproducible and significant in three independent experiments (p < 0.01 by two-way ANOVA). These results further confirm that PAR bZip genes are important for the proper phase of expression of *Cry1*.

## Strength of Intronic RREs Correlates with Phase Delay

To determine whether the strength of RREs in 336 bp of *Cry1* first intron sequence correlates with the phase delay, we generated an array of intron sequences harboring mutant RREs, including deletion, mutation, and inversion of the two RREs (Figure 3A). We inserted these mutant intron sequences into P(SV40)-*Luc* vector to generate an array of P(SV40)-*Cry1* intron 336-*Luc* reporter constructs. As one measurement for the strength of intronic RREs, we first examined transcriptional activation of these constructs by RORα, an activator of RRE, in a reporter assay. We found that induced *Luciferase* activities varied significantly among constructs, ranging from strong induction by wild-type RRE to almost no induction by double-mutant or deleted RREs (R1 and R2) (Figure 3B). These results indicate that the RREs within the intron sequence are functionally responsive to RORα and that intronic RREs of various strengths can be obtained from different RRE mutations.

As an independent measurement for the strength of intronic RREs, we next examined the amplitude of circadian oscillations expressed by these constructs in reporter rhythm assays (Figure S3A and Table S1). Rhythm amplitude was low when an intron sequence of low RORα responsiveness was used to drive reporter expression and high when an intron sequence of high RORα responsiveness was used (Figures 3B and 3C). Overall, there was a significant positive correlation between the two measurements for the strength of intronic RREs: RORα responsiveness and rhythm amplitude among the intronic RRE mutants (r^2 = 0.95, p < 0.01; Figure 3D).

These mutant intron sequences allowed us to analyze quantitatively the role of intronic RREs in the phase delay mechanism. Specifically, we examined how intronic RRE mutation affects phase delay using a reporter rhythm assay (Figure 3E, Figure S3B, and Table S1). We found that the observed phase delay significantly correlated with the first measurement for the strength of the intronic RRE mutants, i.e., RORα responsiveness (r^2 = 0.82, p < 0.01; Figure 3F, top). Similarly, phase delay also correlated well with the second measurement for the strength of the intronic RRE mutants, i.e., the rhythm amplitude (r^2 = 0.90, p < 0.01; Figure 3F, bottom). Taken together, these data suggest that the strength of RREs correlates with the phase delay, further corroborating our finding that the RREs in the *Cry1* intron act as an enhancer to further delay the phase conferred by *Cry1* promoter.

Combination of Day- and Night-Time Elements Produces Evening Phase Control

Given that the delayed expression of *Cry1* is a combined effect of its promoter and intron, we sought to understand whether this combinatorial effect is a general design principle in the circadian transcriptional network or a mechanism unique to the transcriptional regulation of *Cry1*. We first asked whether the phase of endogenous *Cry1* expression could be synthesized using an artificial promoter in clock cells. We constructed three sets of reporters, with each harboring one of the three CCEs (i.e., E/E′ box, D box, and RRE) in the presence or absence of the RRE-containing intron sequence from the *Cry1* gene (Figures 4A and 4B). Real-time bioluminescence recording of transfected NIH 3T3 cells showed that the RRE-containing *Cry1* intron sequence, as expected, did not dramatically alter the phase of
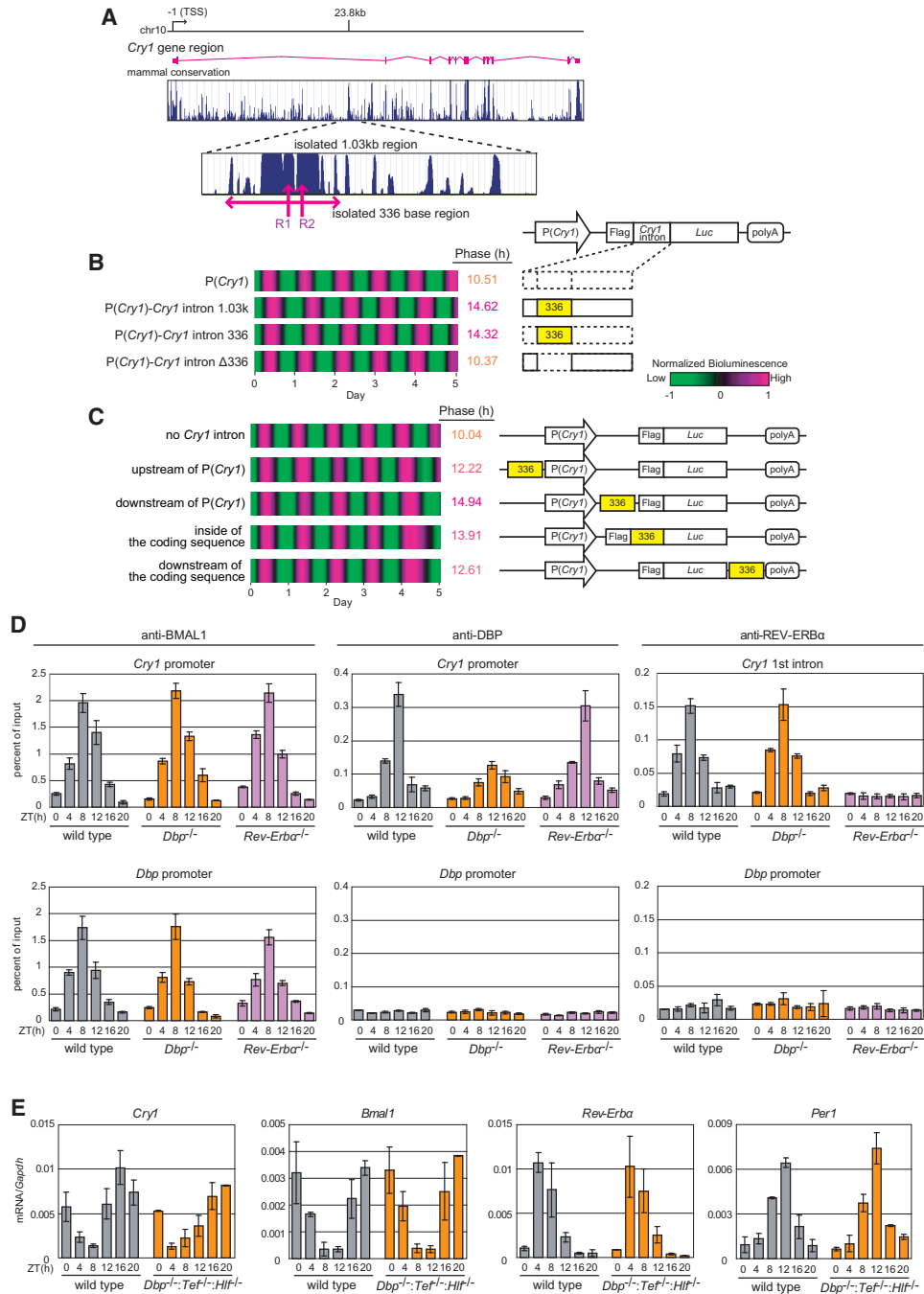
Figure 2. *Cry1* Intron Acts as an Enhancer to Confer Phase Delay

(A) The first intron of *Cry1* contains RRE sequences. The marked 1.03 kbp and 336 bp of *Cry1* first intron sequence, which are highly conserved in mammals, were cloned and examined in this study. Two RREs are indicated as R1 and R2, respectively.

(B) *Cry1*'s first intron confers phase delay. The *Cry1* promoter was combined with the *Cry1* 1.03 kbp intron, 336 bp intron, or *Cry1* intron Δ336 deletion mutant to generate composite promoters. The experiment was performed as in Figure 1A.

(C) *Cry1*'s first intron sequence confers phase delay independently of its location. The 336 bp of *Cry1* intron sequence was inserted upstream or downstream of the *Cry1* promoter and inside or downstream of the coding sequence. Data are representative of two independent experiments (B and C).

(D) Binding of BMAL1 (an E/E′ box regulator) and DBP (a D box regulator) to the *Cry1* promoter region and REV-ERBα (a RRE regulator) to the *Cry1* first intron region in vivo. Chromatin from wild-type (gray), *Dbp*$^{-/-}$ (orange), or *Rev-Erbα*$^{-/-}$ (purple) mice was prepared at 4 hr intervals from mice held in a 12 hr light/12 hr dark cycle (LD 12:12). The binding of each regulator to its regulatory region was analyzed by ChIP with the indicated antibodies. Note that DBP binding in *Dbp*$^{-/-}$ mice was significantly reduced (p < 0.01 by two-way ANOVA), with residual signals potentially deriving from TEF and/or HLF binding. Specific TaqMan probes

RRE-mediated reporter expression, albeit with an increase in amplitude (Figure S4). The intron sequence sometimes caused double peaks for the E′ box-driven rhythms (Figure 4A and Figure S4). When these rhythms were fitted to a circadian cosine curve, we observed a reduction of the relative amplitude and a slight but reproducible phase advance (Figure 4A, Figure S4, and Table S1). Importantly, the combination of D box in the promoter and RRE-containing *Cry1* intron sequence conferred a substantial phase delay of > 5 hr (CT14.48 ± 0.21) when compared to the D box alone (CT9.31 ± 0.16) (Figure 4, Figure S4, and Table S1). It is important to note that our result indicates that E/E′ boxes are dispensable for the generation of delayed-phase expression of *Cry1*. This is because the synthetic composite "D box + RRE" promoter (i.e., a combination of a synthetic D box-driven promoter and RRE-containing *Cry1* intron sequence) lacks functional E boxes, unlike the *Cry1* promoter. Thus, the D box and the RRE can combine to generate a distinct intermediate phase.

We were able to recapitulate these experimental measurements in a simple model using "phase vectors." A phase vector represents phase and amplitude of the oscillation as direction and length of the vector in polar coordinates. In this way, the combination of two oscillations can be represented by the vector sum of two corresponding phase vectors (Extended Experimental Procedures). We plotted measured oscillations (CCE without intron sequence and intron sequence without CCE) and obtained the summed phase vector of the CCE-intron sequence combinations (Figure 4B, left three circles). Interestingly, the summed phase vectors corresponded well with the measured oscillations (Figure 4B, rightmost). These results support the notion that combining two CCEs that otherwise function independently can be a general mechanism for generation of new phases and, more specifically, the combined phase may be predicted, to a first-order approximation, by a vector sum.

Delayed Expression of *Cry1* Restores Circadian Rhythmicity in *Cry1⁻/⁻:Cry2⁻/⁻* Cells

To address the functional importance of the RRE-mediated phase delay, we employed cell-based genetic complementation, testing for phenotypic rescue in arrhythmic *Cry1⁻/⁻:Cry2⁻/⁻* cells. We hypothesized that, if phase delay is an important property of *Cry1*, its delayed expression, peaking at evening-time, should restore circadian oscillations in these cells. To test this hypothesis, we established mouse embryonic fibroblasts from *Cry1⁻/⁻:Cry2⁻/⁻* double-knockout mice (van der Horst et al., 1999). Similar to negative control (Figure 5A, without *Cry1*), *Cry1* expression driven only by the *Cry1* promoter, P(*Cry1*), did not rescue circadian oscillations in these cells (Figure 5A, P(*Cry1*)). However, when *Cry1* expression was regulated by

P(*Cry1*)-*Cry1* intron 336, which contains the *Cry1* promoter and the RRE-containing 336 bp of *Cry1* intron sequence, its exogenous expression restored circadian rhythmicity in these cells, with a period length of 26.73 ± 0.19 hr (Figure 5A, *Cry1* intron 336). The observed rescue capability was independent of the CRY1 protein level, vector type, or method of DNA delivery (Figures S5A and S5B). Taken together, these results demonstrate that delay of *Cry1* expression, conferred by the *Cry1* intron, is required for rescue of circadian rhythmicity.

To further assess the contribution of delayed *Cry1* expression to the rescued circadian oscillation, we tested the rescue capability of the intronic RREs mutants that possess different RRE strengths, as described above (Figure 3 and Figure 5A, nine panels on the right, and Table S2). The ability of the intronic RRE mutants to rescue rhythmicity, represented as amplitude of circadian oscillations, significantly correlated with the strength of intronic RREs, as measured by bioluminescence levels derived from P(*SV40*)-*Cry1* intron 336-*Luc* (r^2 = 0.87, p < 0.01; Figure 5B, left). Similarly, the rescue capability also correlated with another measurement of strength of intronic RREs, i.e., RORα responsiveness of the intronic RRE mutants (r^2 = 0.97, p < 0.01; Figure 5B right). More directly, the rescue capability correlated with the phase delay conferred by the intronic RRE mutants that was measured in bioluminescence rhythms of P(*Cry1*)-*Cry1* intron 336-*Luc* (r^2 = 0.71, p < 0.01; Figure 5C). It should be noted that the rescue capability in these experiments does not correlate with either amplitude or basal bioluminescence levels of P(*Cry1*)-*Cry1* intron 336-*Luc* (Figure S5C), suggesting that the rescue capability is most likely attributable to the delayed phase of *Cry1* expression conferred by RREs. To directly confirm this, we demonstrated that the pure RREs, when combined with *Cry1* promoter, rescued circadian rhythmicity in *Cry1⁻/⁻:Cry2⁻/⁻* cells, whereas *Cry1* promoter alone could not reliably rescue rhythms (Figure S5D and Figure 5).

The *Cry1*-rescued *Cry1⁻/⁻:Cry2⁻/⁻* cells (a *Cry2* knockout, in essence) showed a rather long period length of ~27 hr (Figure 5A), which is consistent with previous reports showing that *Cry2⁻/⁻* single-knockout cells display long periods compared to wild-type cells (~24–25 hr) (Liu et al., 2007). We confirmed that genetic complementation of *Cry1* in *Cry1⁻/⁻:Cry2⁻/⁻* cells recapitulates the circadian phenotype in *Cry2* single-knockout cells, thus phenotypically validating the *Cry1* rescue assay (Figure S5E and Table S3).

Cry1 Phase Delay Modulates Circadian Period Length

The genetic complementation assay expressing *Cry1* of various phases revealed that delay of *Cry1* expression is required to restore circadian rhythmicity, consistent with the proposed design principle for circadian clocks, i.e., transcriptional/translational

---

were used to detect the *Cry1* promoter region, the *Cry1* first intron region, or the *Dbp* promoter region (control region). ZT, Zeitgeber time. Mean and SD represent three ChIP experiments.

(E) Circadian expression profiles of *Cry1*, *Bmal1*, *Rev-Erbα*, and *Per1* in vivo. RNA from liver of wild-type (gray) or *Dbp⁻/⁻:Tef⁻/⁻:Hlf⁻/⁻* (orange) mice was prepared at 4 hr intervals from mice held in LD 12:12 cycle. Relative mRNA levels of each gene were measured. Note that *Cry1* expression in *Dbp⁻/⁻:Tef⁻/⁻:Hlf⁻/⁻* mice was different from wild-type and its peak delayed. All RNA samples were normalized to *Gapdh* mRNA accumulation. Mean and SEM from two pools of three mice each per time point. The representative data from three independent experiments was shown. The observed peak delay was reproducible and significant in three independent experiments (p < 0.01 by two-way ANOVA).

See also Figure S2 and Table S1.
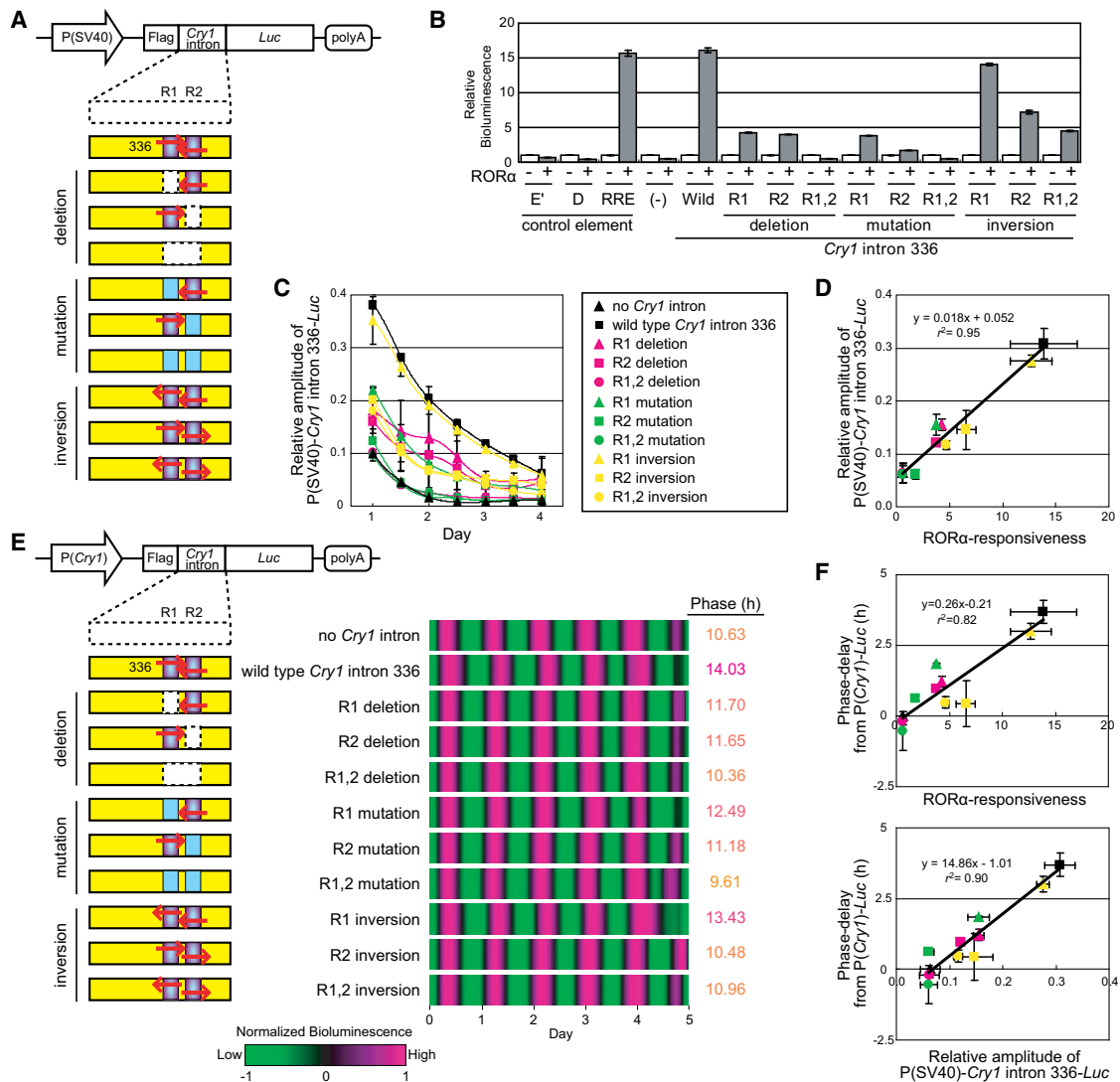
Figure 3. The Strength of Intronic RREs Correlates with Phase Delay

(A) Mutant reporter constructs derived from P(SV40)-*Cry1* intron 336-*Luc*. P(SV40)-*Cry1* intron 336-*Luc* contains the 336 bp of *Cry1* intron sequence (wild-type); the RREs or R1/R2 within the *Cry1* intron sequence were altered to generate three sets of *Cry1* intron sequence mutants: deletions, mutations, and inversions. Red arrow indicates the direction of R1 and R2. Purple, light blue, and white rectangles represent wild-type, mutated, and deleted RREs, respectively.

(B) RORα responsiveness of mutated intron sequences. Each reporter construct in (A) was transiently transfected into NIH 3T3 cells in the absence (–) or presence (+) of RORα. *Luciferase* activities were scaled so that basal activity without RORα was 1.

(C) Relative amplitudes of circadian transcriptional activities induced by constructs presented in (A).

(D) Correlation between two measurements for the strength of intronic RREs, the RORα responsiveness (B), and the relative rhythm amplitude (C) of mutated intron sequences.

(E) Mutant reporter constructs derived from P(*Cry1*)-*Cry1* intron 336-*Luc* and their phases. The SV40 promoter in P(SV40)-*Cry1* intron 336-*Luc* was replaced with *Cry1* promoter P(*Cry1*) to generate P(*Cry1*)-*Cry1* intron 336-*Luc*. The RRE mutations in P(*Cry1*)-*Cry1* intron 336-*Luc* are the same as in P(SV40)-*Cry1* intron 336-*Luc* constructs in (A).

(F) Phase delay correlates with two measurements for the strength of intronic RREs, the RORα responsiveness and the relative rhythm amplitude. The RORα responsiveness presented in (B) (top) and relative rhythm amplitudes presented in (C) (bottom) of mutated intron sequences are plotted against phase delay of P(*Cry1*)-*Cry1* intron 336-*Luc* activity relative to P(*Cry1*)-*Luc* activity presented in (E).

Data are representative of two independent experiments (B, C, and E). Error bars represent SD (n = 3) (B and C). Mean and SD (error bar) of two independent experiments are shown (each experiment contains three samples; n = 3 unless otherwise indicated in Table S1) (D and F). See also Figure S3 and Table S1.

feedback repression with delay. This design principle further predicts that *Cry1* expression with a more prolonged delay can slow circadian oscillations. To test this prediction, we first attemp-

ted to generate constructs expressing *Cry1* with prolonged delays. According to the phase-vector model described above (Figure 4B), we should be able to generate evening-to-night
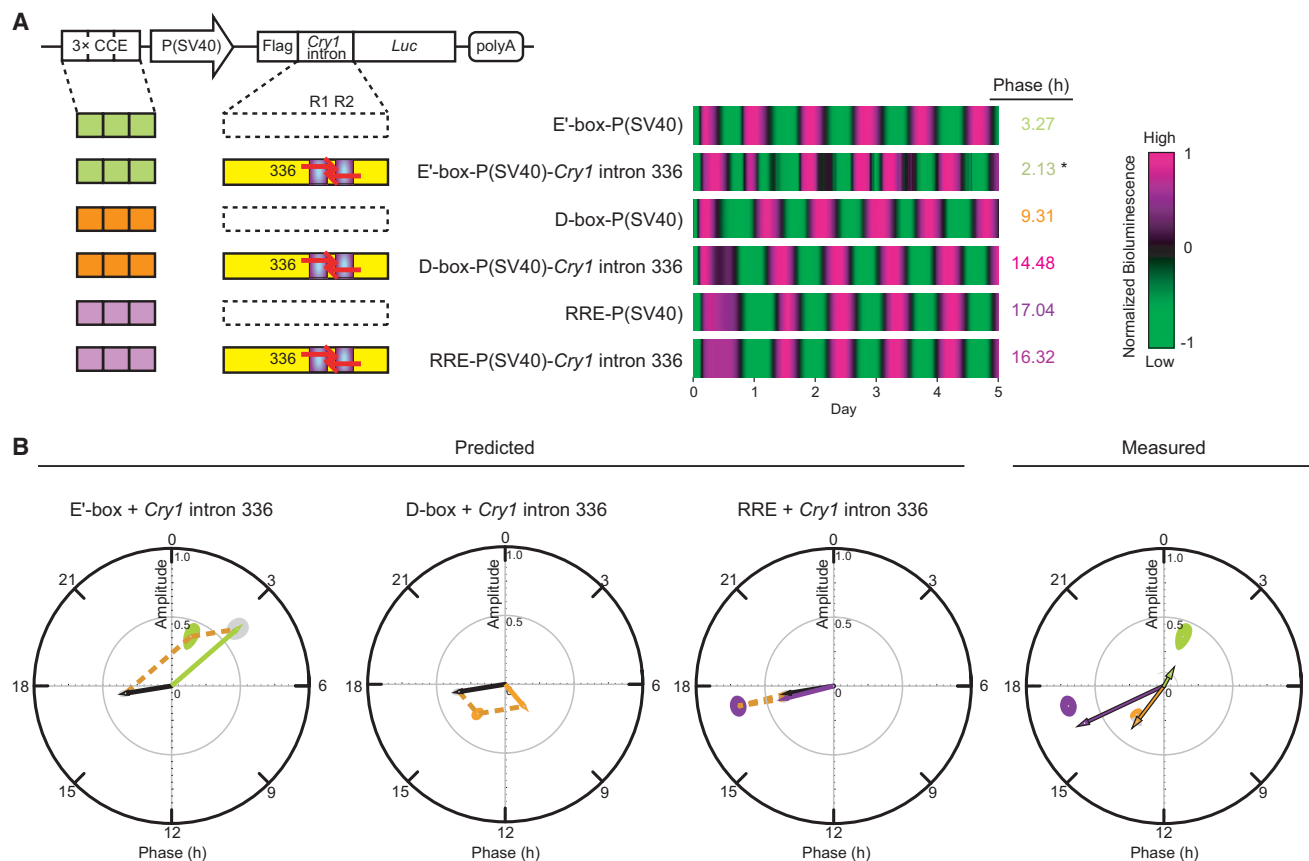
Figure 4. Combination of Intronic RREs with Known Circadian *cis*-Elements Gives Rise to Emergent Phases that Can Be Predicted by Phase Vectors

(A) Combination of the *Cry1* intron sequence with known CCEs gives rise to emergent phases. A promoter was constructed by inserting 3 × E′ box, 3 × D box, or 3 × RRE sequences in the upstream of P(SV40). In the reporter construct, *Luciferase* expression was under the control of the 3 × CCE-P(SV40) promoter in the absence or presence of the 336 bp of *Cry1* intron sequence. The experiment was performed as in Figure 1A. Phases were estimated by fitting a cosine wave with circadian period corresponding to maximum autocorrelation of the time series using detrended bioluminescence data. This method allowed phase estimation of even distorted wave form expressed by E′ box + *Cry1* intron sequence (marked by asterisk).

(B) A phase vector model recapitulates the emergent phases. The phase vector of each CCE (E′ box, green arrow; D box, orange arrow; RRE, purple arrow) and *Cry1* intron sequence (black arrow) and the vector sum of the two phase vectors (center of colored ellipsoid) are plotted in the polar coordinate (left three circles). The ellipsoidal disk represents 95% confidence region. The phase vectors (colored arrows of black border) represent measured circadian transcriptional activities induced by the combined regulation of *Cry1* intron sequence and each CCE (rightmost circle).

Data are representative of two independent experiments. See also Figure S4 and Table S1.

expression with a more prolonged delay by weakening the day-time promoter but keeping a constant strength of the night-time enhancer of *Cry1* intron sequence. Therefore, we generated an array of day-time promoters with various strengths of D boxes, containing 1, 2, or 3 tandem repeats of D boxes or Cry1proD elements; we confirmed that these day-time promoters displayed day-time phased bioluminescence rhythms of various relative amplitudes, as expected (Figure 6A, Figure S6A, and Table S1). We then generated another set of constructs by combining these day-time promoters with the *Cry1* intron sequence (Figure 6B, Figure S6B, and Table S1). These constructs displayed evening-to-night phases of bioluminescence rhythms (Figure 6B, Figure S6B, and Table S1). Importantly, there was a significant correlation between the observed phases and the predicted phases from the simple phase-vector model (r^2 = 0.77, p < 0.01; Figure 6C, rightmost panel).

Next, we asked whether evening-to-night *Cry1* expression with prolonged delay could slow circadian oscillations (Figure 6D and Table S3). Interestingly, the periods of rescued circadian oscillations ranged from 27 to 31 hr. In particular, period length correlated with the delay prolonged by weakening the day-time promoter: the more the *Cry1* phase was delayed, the longer the rescued period (r^2 = 0.81, p < 0.01; Figure 6E and see also Figure S6C). We also confirmed that the period length did not significantly correlate with either amplitude or basal activity of *Cry1* expression by using a different constitutive promoter (Figure S6D and Table S3). In addition, CRY1 protein level was not responsible for the changes in rescued period (Figure S6E). These results showed that *Cry1* expression with a prolonged delay slows circadian oscillations, further supporting the proposed design principle of circadian clocks—transcriptional/translational feedback repression with delay.
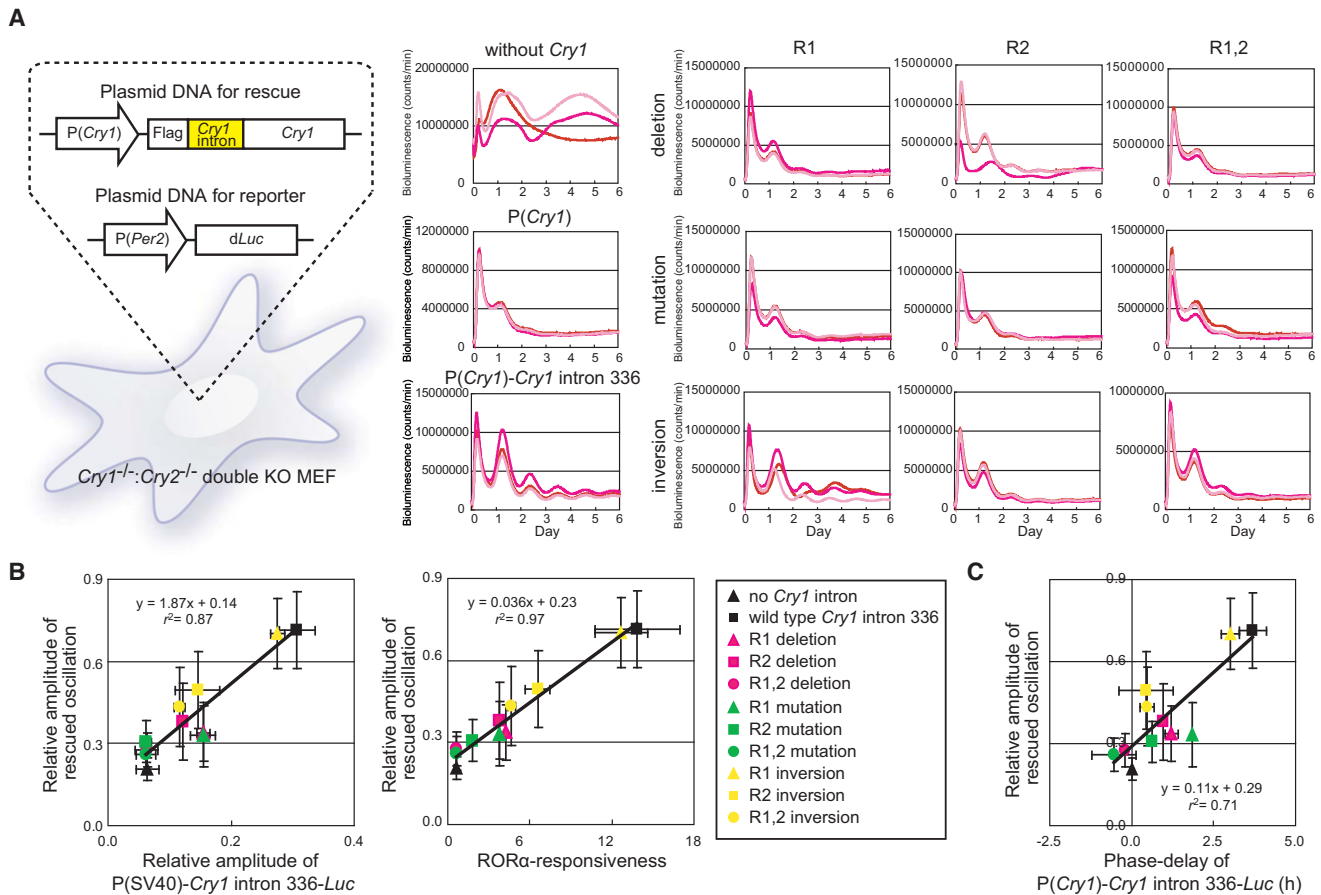
Figure 5. Delayed Expression of *Cry1* Restores Circadian Rhythmicity in *Cry1*^{−/−}:*Cry2*^{−/−} Cells

(A) Genetic complementation of *Cry1* rescues circadian oscillation in *Cry1*^{−/−}:*Cry2*^{−/−} cells. A schematic diagram of *Cry1* rescue constructs is shown on the left. The composite promoter contains P(*Cry1*) and the 336 bp *Cry1* intron sequence of wild-type or a mutant (deletion, mutation, or inversion of the R1 and R2 sequences as in Figure 3), which controls *Cry1* expression. *Cry1* rescue constructs were each cotransfected with a destabilized *Luciferase* reporter construct, P(*Per2*)-d*Luc*, into *Cry1*^{−/−}:*Cry2*^{−/−} mouse embryonic fibroblast cells (left), followed by bioluminescence recording. Whereas mock-transfected *Cry1*^{−/−}:*Cry2*^{−/−} cells were completely arrhythmic and those expressing P(*Cry1*)-*Cry1* were only transiently rhythmic during the first 2 days of recording, P(*Cry1*)-*Cry1* intron 336-*Cry1* expression restored circadian oscillation with a period length of 26.73 ± 0.19 hr (bottom in the center column). Rescue effects varied among the intronic RRE mutants (right nine panels). Data are representative of two independent experiments.

(B) Relative amplitude of rescued circadian oscillation correlates with the strength of intronic RREs. The relative amplitudes of rescued oscillation are plotted against two measurements for the strength of intronic RREs, the relative amplitudes of P(SV40)-*Cry1* intron 336-*Luc* oscillation presented in Figure 3C, and the RORα responsiveness presented in Figure 3B.

(C) Relative amplitude of rescued circadian oscillation correlates with phase delay. The relative amplitudes of rescued oscillations are plotted against the phase delay of various P(*Cry1*)-*Cry1* intron 336-*Luc* activities relative to P(*Cry1*)-*Luc* activity presented in Figure 3E.

Mean and SD (error bar) of two independent experiments are shown (each experiment contains three samples; n = 3 unless otherwise indicated in Table S1). See also Figure S5 and Table S2.

Single-Cell Analysis Confirms the Importance of *Cry1* Phase Delay in Feedback Repression

Arrhythmic phenotypes observed in population of cells might be due to rapid damping of individual cells or lack of synchronization among individual cells. To discriminate between these possibilities, we monitored bioluminescence levels in real time at the level of single-cell resolution (Sato et al., 2006; Ukai et al., 2007). As with whole-well assays, single-cell analysis showed that most individual cells expressing *Cry1* with a normal delay, driven by the intron sequence containing wild-type RREs, were robustly rhythmic, with a circadian period of 26.77 ± 0.12 hr

(Figures 7A and 7B and Table S3), whereas most cells expressing *Cry1* without delay, driven by an intron sequence harboring mutated RREs, were arrhythmic (Figure 7B and Movie S1). Moreover, individual cells expressing *Cry1* with a prolonged delay driven by the *Cry1* intron sequence alone (i.e., in the absence of *Cry1* promoter) displayed long circadian periods of up to 32.00 ± 0.58 hr (Figures 7A and 7B and Table S3). The circadian oscillations in Figure 7A with delayed *Cry1* expression were statistically significant (p < 0.01 by autocorrelation) and reproducible in different series of experiments. Thus, single-cell analysis confirmed the circadian phenotypes observed in
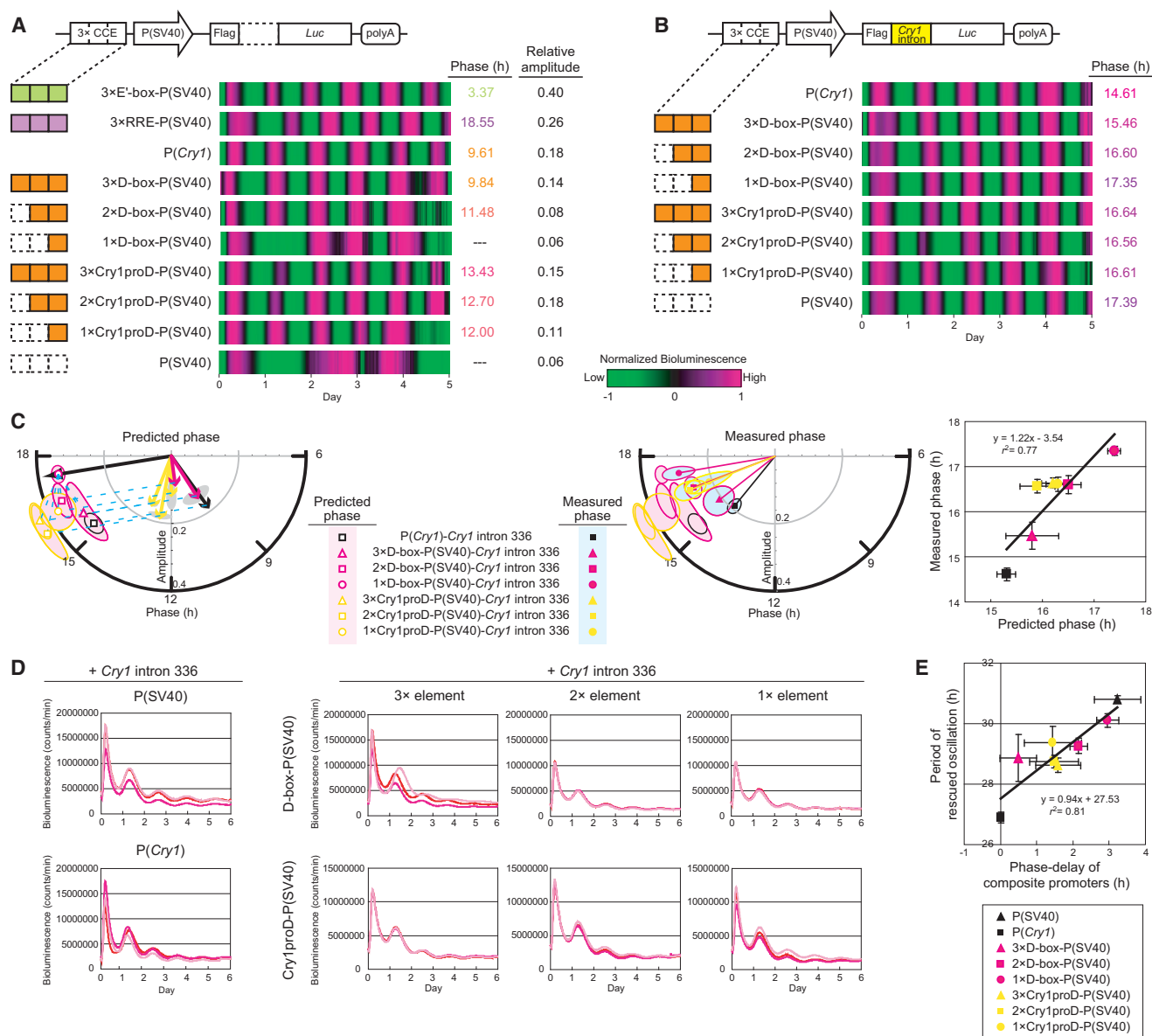
Figure 6. Prolonged Delay of *Cry1* Expression Slows Circadian Oscillations in *Cry1*^{−/−}:*Cry2*^{−/−} Cells

(A) Promoters harboring various CCEs display different circadian phases. The promoters contain one, two, or three tandem copies of D box or Cry1proD element, which were inserted into the P(SV40)-*Luc* vector to generate an array of reporter constructs.

(B) The 336 bp of *Cry1* intron sequence confers phase delay to D box and Cry1proD element. Reporter constructs were generated similarly as in (A) except that the 336 bp of *Cry1* intron sequence was inserted. The experiment was performed as in Figure 1A (A and B).

(C) The measured phases conferred by the composite promoters are consistent with those predicted by phase vectors. (Left) The phase vectors of oscillations driven by various promoters without the intron sequence (colored arrows) and those driven by the intron sequence (∼CT17.5) or P(*Cry1*) (∼CT10) (two black arrows) are plotted with summed phase vectors (center of colored ellipsoidal disks). The ellipsoidal disk represents 95% confidence region. (Right) The summed phase vectors in the left circle are plotted with phase vectors of measured oscillations driven by the composite promoters. (Rightmost) The predicted phases from the simple phase-vector model are plotted against the observed phases. Error bars represent SD (n = 3).

(D) *Cry1* rescue of circadian oscillation in *Cry1*^{−/−}:*Cry2*^{−/−} cells using synthetic composite promoters. The composite promoters presented in (B) were used to drive *Cry1* expression. *Cry1*^{−/−}:*Cry2*^{−/−} cells were cotransfected with a *Cry1* expression construct and a P(*Per2*)-d*Luc* reporter.

(E) Prolonged phase delay of *Cry1* expression correlates with period length of rescued oscillations. The period lengths of rescued oscillations are plotted against the phase delay of various composite promoters' activity relative to P(*Cry1*)-*Cry1* intron 336-*Luc* activity presented in (B). Mean and SD (error bar) of two independent experiments are shown (each experiment contains three samples; n = 3).

Data are representative of two independent experiments (A, B, and D). See also Figure S6, Table S2, and Table S3.
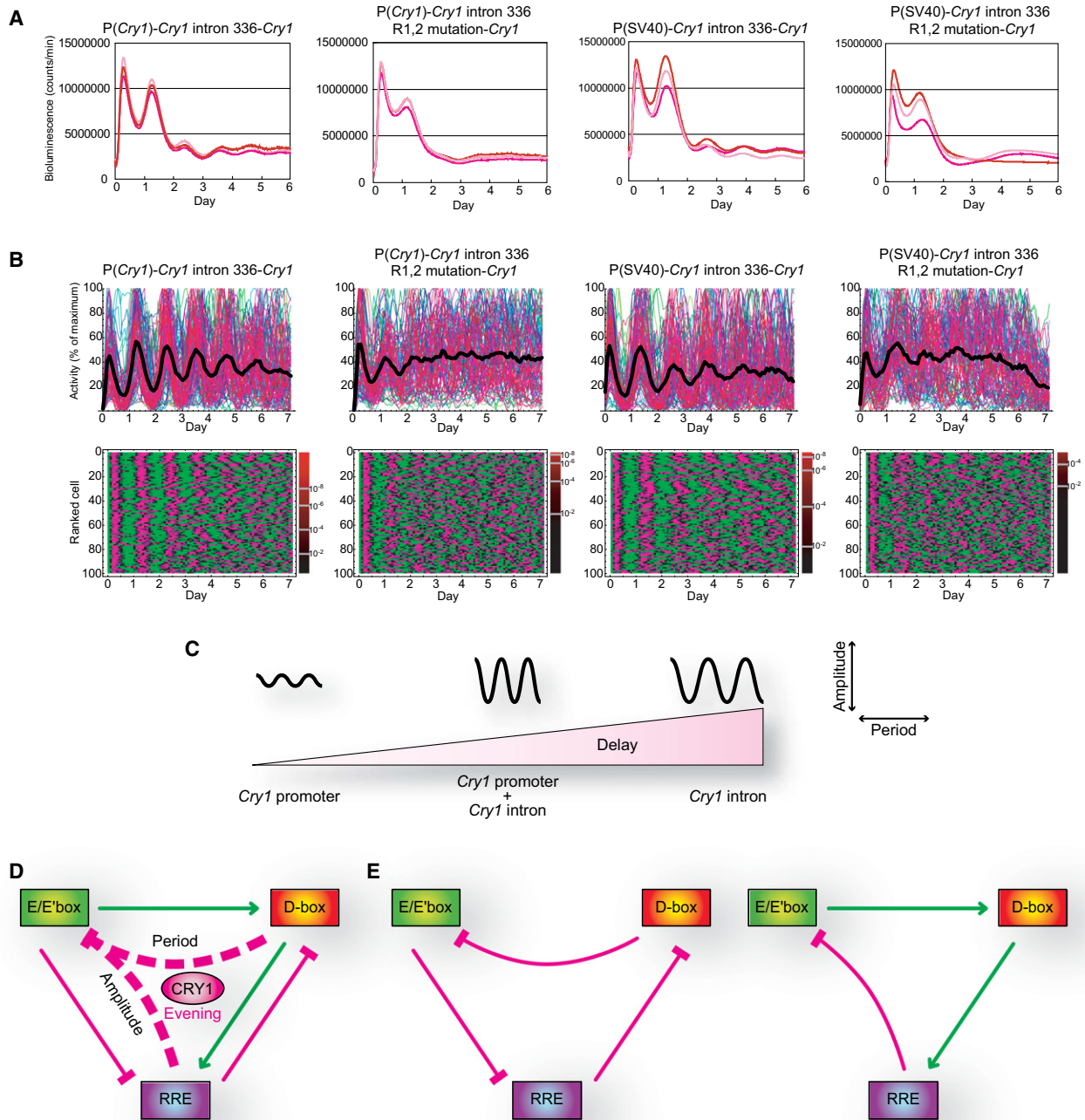
Figure 7. Single-Cell Analysis Confirms the Requirement of *Cry1* Phase Delay

(A) P(*Per2*)-d*Luc* bioluminescence levels in transfected *Cry1*$^{-/-}$:*Cry2*$^{-/-}$ cells as recorded. The P(*Per2*)-d*Luc* reporter and a *Cry1* expression construct as indicated were cotransfected into *Cry1*$^{-/-}$:*Cry2*$^{-/-}$ cells, and bioluminescence expression was recorded with a PMT. Data from three independent samples are shown.

(B) P(*Per2*)-d*Luc* bioluminescence levels in transfected individual *Cry1*$^{-/-}$:*Cry2*$^{-/-}$ cells as recorded by a luminescence microscope (n = 100). Reporter activities from each cell were normalized so that the maximum and minimum bioluminescence values are 100% and 0%, respectively. The mean reporter activity for all of the analyzed single cells at each time point is indicated by a thick black line (top row). Time series of bioluminescence expression shown in the top row were redrawn as heatmaps (bottom row). Each row in the heatmap represents a time series of P(*Per2*)-d*Luc* reporter activities from a single cell. The corresponding p value of rhythmicity at the period of maximum autocorrelation was evaluated for each time series and is depicted on the right. One-hundred cells were randomly selected and individually analyzed. Data are representative of two independent experiments (A and B).

(C) The roles of phase delay in *Cry1* expression. Through regulation of *Cry1* expression, the promoter and intron primarily affect the amplitude and period of the clock system, respectively.

Cry1-rescued *Cry1*⁻/⁻:*Cry2*⁻/⁻ cells at the cell population level, which lends strong support for our finding that delay of *Cry1* expression is required for circadian clock function.

DISCUSSION

Cry1 Phase Control Mechanism
In this report, we provided experimental data, as well as model predictions, for a "combinatorial regulatory mechanism" to explain the delayed expression of *Cry1*. We newly identified D boxes, which overlap with the E/E′ box and confer phase delay over E/E′ box activity. In addition, we also demonstrated that the previously identified RREs in the first intron (Ueda et al., 2005) can confer the additional phase delay in *Cry1* expression. Furthermore, we observed that the synthetic pure RREs, in combination with *Cry1* promoter, rescued circadian rhythmicity in *Cry1*⁻/⁻:*Cry2*⁻/⁻ cells with statistical significance (p < 0.01; Figure S5D). Together with the observation that the combination of pure D box and *Cry1* intron sequence also rescued rhythms (Figure 6D), we conclude that the RRE and D box elements can recapitulate the basic function of *Cry1* intron and *Cry1* promoter, respectively. It should be noted that the possible contribution from unknown elements in *Cry1* intron 336 sequence could not be completely excluded because the relative amplitude of the pure RRE elements (combined with *Cry1* promoter) is slightly lower than that of the wild-type *Cry1* intron 336 (combined with *Cry1* promoter, Figure S5D).

General Design Principles for New Phases
As revealed in this study, these multiple distinct regulatory sites (i.e., two RREs in first intron and the E/E′ box and D boxes in the promoter region) function in a coordinated fashion to generate substantial phase delay, leading to evening-time expression. Interestingly, in an effort to study design principles of the circadian clockwork, we employed a simple phase-vector model in which the new evening-time could be predicted by the combination of two component phase vectors. Although the phase-vector model was not used for phase prediction in our previous study (Ukai-Tadenuma et al., 2008), such a model is also applicable to this previous study when we take into account the time delay associated with transcription/translation of regulator proteins and the *Luciferase* reporter ($r^2 = 0.99$, p < 0.01; Figures S7A and S7B and Table S4). These results show that a new phase can be generated through combinatorial synthesis of either two transcriptional regulators or two clock-controlled DNA elements and also can be described, at least to a first-order approximation, by a phase-vector model. Taken together, this combinatorial regulatory mechanism for the generation of new circadian phases of transcription represents a general design principle underpinning the complex system behavior.

Although the phase-vector model predicts the phase of a synthesized oscillation, it is only a first-order approximation.

For example, there are some discrepancies between predicted and measured amplitudes. Also, the wave form generated by the combination of E′ box-driven promoter and the *Cry1* intron sequence appeared like a "two-peak" wave form (Figure S4, upper-left), indicative of nonlinear effects or involvement of yet unknown factors. In detailed analysis, we found that the ∼11 hr period oscillation was actually a significant component in the two-peak wave form (Figure S4, upper-right; p < 0.01). This is the first demonstration of synthesized ultradian rhythms, which may lead to insights into mechanisms of ultradian gene expression with harmonic periods, as recently reported (Hughes et al., 2009).

Delayed *Cry1* Expression Contributes to Clock Robustness
In this study, we focused on the level of transcriptional regulation and demonstrated the importance of delay in feedback repression at the intracellular level. Constitutive expression of *Cry1* abolished circadian rhythmicity in wild-type cells (Ueda et al., 2005) and failed to restore circadian oscillation in arrhythmic *Cry1*⁻/⁻:*Cry2*⁻/⁻ cells (Figure S6D and Figure 7A), suggesting that rhythmic expression of *Cry1* is important for clock function. We revealed that the transcriptional oscillation of *Cry1* with a correct phase with substantial delay was sufficient and required to rescue circadian oscillation in arrhythmic *Cry1*⁻/⁻:*Cry2*⁻/⁻ cells (Figure 5) and that transcriptional oscillation of *Cry1* with a prolonged delay slows circadian oscillation (Figure 6). Importantly, we also confirmed that the amount (baseline) of CRY1 protein was not responsible for the changes in amplitude (Figure S5A) and period (Figure S6E) of rescued oscillations. These results suggest that the phase of *Cry1* expression is responsible for the changes in rescued amplitude and period rather than the amount (baseline) of CRY1 protein. Because we confirmed the significant linear correlation between transcriptional activities and protein levels (p < 0.01), when monitored by firefly *Luciferase*, and CRY1 protein amounts, when monitored by fusion *Renilla Luciferase*, irrespective of cell types ($r^2 = 0.93$ in NIH3T3 and $r^2 = 0.90$ in *Cry1*⁻/⁻:*Cry2*⁻/⁻ cells), we speculated that phase of CRY1 protein level would be responsible for the amplitude and period of rescued oscillations.

It should be noted that the CRY1 protein expression levels in our experiments are within a certain range (Figure S5A and Figure S6E), and we do not exclude (and our current results are not in conflict with) the notion that CRY1 protein amounts may affect the parameters of clock function when CRY1 protein levels drastically differ from those in our experimental system, as previously reported (Baggs et al., 2009; Ueda et al., 2005). In addition, we do not exclude the possibility that other regulatory mechanisms such as posttranscriptional modifications (Lee et al., 2001; Liu et al., 2008) play important roles in attaining the robustness of the clock. For example, rhythmic expression of PER2 is recently reported to play a prominent role in CRY1 function (Chen et al.,

(D) A schematic diagram of a minimal circuit for the mammalian circadian transcriptional network. The network can be represented by a simple circuit, consisting of two transcriptional activations (green arrows) and four transcriptional repressions (red arrows) on three regulatory elements (three rectangles).
(E) The minimal circuit envisaged as a composite of two distinct oscillatory network motifs: (1) A repressilator that is composed of three repressions (left) and (2) a delayed negative feedback loop, which is composed of two activations and one repression (right). See also Figure S7, Movie S1, and Table S3.

2009). And PER2 is phosphorylated by CKIδ/ε, which is also an essential mammalian clock component (Lee et al., 2009) and has been recently implicated in temperature compensation (Isojima et al., 2009). In addition, it has been reported that constant supply of membrane-permeable CRY1 and CRY2 proteins rescued circadian oscillation in $Cry1^{-/-}:Cry2^{-/-}$ cells (Fan et al., 2007). In line with this observation, our single-cell analysis indicated that a fraction of individual cells transfected with Cry1 driven by a constitutive promoter exhibited weak circadian oscillation even though the rhythms are rather transient (Figure 7B), implying that constant Cry1 expression might partially rescue circadian clock function. This qualitatively less-robust clock function is probably attributable to posttranscriptional and posttranslational mechanisms (Lee et al., 2001; Liu et al., 2008).

Even in this context, it appears that phase delay in rhythmic Cry1 expression may contribute to the robustness of clock function by ensuring properly timed nuclear translocation of CRY proteins. This idea is strongly supported by our results presented in this study: delayed Cry1 expression via D box-mediated transcription (i.e., from Cry1 promoter) allowed partial rescue, and further delay via the RREs from the Cry1 intron restored circadian rhythmicity with amplitude and persistence comparable to wild-type cells.

Design Principle for a Circadian Transcriptional Network
Delayed feedback repression is one of the most prevailing but as yet unverified design principles for a circadian transcriptional network. This design principle predicts that decreased delay dampens circadian oscillations and that prolonged delay slows down circadian oscillations (Figure 7C, Figures S7C–S7F, and Extended Experimental Procedures) (Bernard et al., 2006; Lewis, 2003; Novak and Tyson, 2008). The results presented in this study are consistent with the two predictions from the delayed feedback repression, suggesting that it is an applicable design principle in the mammalian circadian transcriptional network.

A Minimal Circuit for a Circadian Transcriptional Network
In a previous effort to identify a minimal circuit of the complex autoregulatory transcriptional networks in the mammalian circadian clock, we showed that day-time promoter activity can be reconstructed by combining a morning-time activator and a night-time repressor and night-time promoter activity by combining a day-time activator and a morning-time repressor (Ukai-Tadenuma et al., 2008). In this study, we succeeded in synthesizing the evening-time phase control of transcription. Our previous and current results suggest that the complex mammalian transcription network can be reduced to a relatively simple diagram (Figure 7D) that would consist of three regulatory elements and six transcriptional regulations (two activations and four repressions). It is noteworthy that this diagram can be envisaged as a composite of two distinct oscillatory network motifs (Figure 7E). The first oscillatory network motif is composed of three repressions (i.e., E/E′ box to RRE, RRE to D box, and D box to E/E′ box), comprising a cyclic negative feedback loop—a repressilator (Elowitz and Leibler, 2000). The second oscillatory network motif is composed of two activations (i.e.,

E/E′ box to D box and D box to RRE) and one repression (i.e., RRE to E/E′ box), comprising a delayed negative feedback loop. It is interesting to note that oscillatory properties of both network motifs were experimentally suggested by synthetic approaches (Elowitz and Leibler, 2000; Stricker et al., 2008). Therefore, further experimental and theoretical analyses of the composite of these oscillatory network motifs lie ahead.

EXPERIMENTAL PROCEDURES

Preparation of Embryonic Fibroblasts from $Cry1^{-/-}:Cry2^{-/-}$ Double-Knockout Mice
$Cry1^{-/-}:Cry2^{-/-}$ double-knockout mice (van der Horst et al., 1999) were carefully kept and handled according to the RIKEN Regulations for Animal Experiments. The dissociated cells (mouse embryonic fibroblasts [MEF] from $Cry1^{-/-}:Cry2^{-/-}$ double-knockout mice; $Cry1^{-/-}:Cry2^{-/-}$ cells) were suspended and cultured in DMEM (Invitrogen) supplemented with 10% FBS (JRH Biosciences) and antibiotics (see Extended Experimental Procedures for details).

Real-Time Circadian Reporter Assay Using NIH 3T3 Cells and $Cry1^{-/-}:Cry2^{-/-}$ Cells
Real-time circadian assays were performed as previously described (Sato et al., 2006; Ueda et al., 2005) with the following modifications. NIH 3T3 cells were transfected with the Luciferase reporter plasmids. $Cry1^{-/-}:Cry2^{-/-}$ cells were transfected with pGL3-P(Per2)-dLuc reporter plasmid (Sato et al., 2006) and each Cry1 gene expression vector. The cells were stimulated by 10 μM (NIH 3T3) or 30 μM ($Cry1^{-/-}:Cry2^{-/-}$ cells) forskolin (Fermentek), and the bioluminescence was measured at 30°C (see Extended Experimental Procedures for details).

SUPPLEMENTAL INFORMATION

ACKNOWLEDGMENTS

REFERENCES

Baggs, J.E., Price, T.S., DiTacchio, L., Panda, S., FitzGerald, G.A., and Hogenesch, J.B. (2009). Network Features of the Mammalian Circadian Clock. PLoS Biol. 7, e1000052.

Bernard, S., Cajavec, B., Pujo-Menjouet, L., Mackey, M.C., and Herzel, H. (2006). Modelling transcriptional feedback loops: the role of Gro/TLE1 in Hes1 oscillations. Philos. Transact. A Math. Phys. Eng. Sci. 364, 1155–1170.

Brown, S.A., Fleury-Olela, F., Nagoshi, E., Hauser, C., Juge, C., Meier, C.A., Chicheportiche, R., Dayer, J.M., Albrecht, U., and Schibler, U. (2005). The period length of fibroblast circadian gene expression varies widely among human individuals. PLoS Biol. 3, e338.

Chen, R., Schirmer, A., Lee, Y., Lee, H., Kumar, V., Yoo, S.-H., Takahashi, J.S., and Lee, C. (2009). Rhythmic PER Abundance Defines a Critical Nodal Point for Negative Feedback within the Circadian Clock Mechanism. Mol. Cell 36, 417–430.

DeBruyne, J.P., Weaver, D.R., and Reppert, S.M. (2007). Peripheral circadian oscillators require CLOCK. Curr. Biol. 17, R538–R539.

Dunlap, J.C. (1999). Molecular bases for circadian clocks. Cell 96, 271–290.

Elowitz, M.B., and Leibler, S. (2000). A synthetic oscillatory network of transcriptional regulators. Nature 403, 335–338.

Etchegaray, J.P., Lee, C., Wade, P.A., and Reppert, S.M. (2003). Rhythmic histone acetylation underlies transcription in the mammalian circadian clock. Nature 421, 177–182.

Falvey, E., Marcacci, L., and Schibler, U. (1996). DNA-binding specificity of PAR and C/EBP leucine zipper proteins: a single amino acid substitution in the C/EBP DNA-binding domain confers PAR-like specificity to C/EBP. Biol. Chem. 377, 797–809.

Fan, Y., Hida, A., Anderson, D.A., Izumo, M., and Johnson, C.H. (2007). Cycling of CRYPTOCHROME proteins is not necessary for circadian-clock function in mammalian fibroblasts. Curr. Biol. 17, 1091–1100.

Fustin, J.M., O'Neill, J.S., Hastings, M.H., Hazlerigg, D.G., and Dardente, H. (2009). Cry1 circadian phase in vitro: wrapped up with an E box. J. Biol. Rhythms 24, 16–24.

Gachon, F., Fonjallaz, P., Damiola, F., Gos, P., Kodama, T., Zakany, J., Duboule, D., Petit, B., Tafti, M., and Schibler, U. (2004). The loss of circadian PAR bZip transcription factors results in epilepsy. Genes Dev. 18, 1397–1412.

Gekakis, N. (1998). Role of the CLOCK protein in the mammalian circadian mechanism. Science 280, 1564–1569.

Griffin, E.A., Jr., Staknis, D., and Weitz, C.J. (1999). Light-independent role of CRY1 and CRY2 in the mammalian circadian clock. Science 286, 768–771.

Harding, H.P., and Lazar, M.A. (1993). The orphan receptor Rev-ErbA alpha activates transcription via a novel response element. Mol. Cell. Biol. 13, 3113–3121.

Hogenesch, J.B., Chan, W.K., Jackiw, V.H., Brown, R.C., Gu, Y.Z., Pray-Grant, M., Perdew, G.H., and Bradfield, C.A. (1997). Characterization of a subset of the basic-helix-loop-helix-PAS superfamily that interacts with components of the dioxin signaling pathway. J. Biol. Chem. 272, 8581–8593.

Hughes, M.E., DiTacchio, L., Hayes, K.R., Vollmers, C., Pulivarthy, S., Baggs, J.E., Panda, S., and Hogenesch, J.B. (2009). Harmonics of circadian gene transcription in mammals. PLoS Genet. 5, e1000442.

Isojima, Y., Nakajima, M., Ukai, H., Fujishima, H., Yamada, R.G., Masumoto, K.H., Kiuchi, R., Ishida, M., Ukai-Tadenuma, M., Minami, Y., et al. (2009). CKIepsilon/delta-dependent phosphorylation is a temperature-insensitive, period-determining process in the mammalian circadian clock. Proc. Natl. Acad. Sci. USA 106, 15744–15749.

Kume, K., Zylka, M.J., Sriram, S., Shearman, L.P., Weaver, D.R., Jin, X., Maywood, E.S., Hastings, M.H., and Reppert, S.M. (1999). mCRY1 and mCRY2 are essential components of the negative limb of the circadian clock feedback loop. Cell 98, 193–205.

Lee, C., Etchegaray, J., Cagampang, F.R., Loudon, A.S., and Reppert, S.M. (2001). Posttranslational mechanisms regulate the mammalian circadian clock. Cell 107, 855–867.

Lee, H., Chen, R., Lee, Y., Yoo, S., and Lee, C. (2009). Essential roles of CKIdelta and CKIepsilon in the mammalian circadian clock. Proc. Natl. Acad. Sci. USA 106, 21359–21364.

Lewis, J. (2003). Autoinhibition with transcriptional delay: a simple mechanism for the zebrafish somitogenesis oscillator. Curr. Biol. 13, 1398–1408.

Liu, A.C., Tran, H.G., Zhang, E.E., Priest, A.A., Welsh, D.K., and Kay, S.A. (2008). Redundant function of REV-ERBalpha and beta and non-essential role for Bmal1 cycling in transcriptional regulation of intracellular circadian rhythms. PLoS Genet. 4, e1000023.

Liu, A.C., Welsh, D.K., Ko, C.H., Tran, H.G., Zhang, E.E., Priest, A.A., Buhr, E.D., Singer, O., Meeker, K., Verma, I.M., et al. (2007). Intercellular coupling confers robustness against mutations in the SCN circadian clock network. Cell 129, 605–616.

Lopez-Molina, L., Conquet, F., Dubois-Dauphin, M., and Schibler, U. (1997). The DBP gene is expressed according to a circadian rhythm in the suprachiasmatic nucleus and influences circadian behavior. EMBO J. 16, 6762–6771.

Mitsui, S., Yamaguchi, S., Matsuo, T., Ishida, Y., and Okamura, H. (2001). Antagonistic role of E4BP4 and PAR proteins in the circadian oscillatory mechanism. Genes Dev. 15, 995–1006.

Novak, B., and Tyson, J.J. (2008). Design principles of biochemical oscillators. Nat. Rev. Mol. Cell Biol. 9, 981–991.

Preitner, N., Damiola, F., Lopez-Molina, L., Zakany, J., Duboule, D., Albrecht, U., and Schibler, U. (2002). The orphan nuclear receptor REV-ERBalpha controls circadian transcription within the positive limb of the mammalian circadian oscillator. Cell 110, 251–260.

Reppert, S.M., and Weaver, D.R. (2002). Coordination of circadian timing in mammals. Nature 418, 935–941.

Ripperger, J.A., and Schibler, U. (2006). Rhythmic CLOCK-BMAL1 binding to multiple E box motifs drives circadian Dbp transcription and chromatin transitions. Nat. Genet. 38, 369–374.

Sato, T.K., Yamada, R.G., Ukai, H., Baggs, J.E., Miraglia, L.J., Kobayashi, T.J., Welsh, D.K., Kay, S.A., Ueda, H.R., and Hogenesch, J.B. (2006). Feedback repression is required for mammalian circadian clock function. Nat. Genet. 38, 312–319.

Stricker, J., Cookson, S., Bennett, M.R., Mather, W.H., Tsimring, L.S., and Hasty, J. (2008). A fast, robust and tunable synthetic gene oscillator. Nature 456, 516–519.

Ueda, H.R., Chen, W., Adachi, A., Wakamatsu, H., Hayashi, S., Takasugi, T., Nagano, M., Nakahama, K., Suzuki, Y., Sugano, S., et al. (2002). A transcription factor response element for gene expression during circadian night. Nature 418, 534–539.

Ueda, H.R., Hayashi, S., Chen, W., Sano, M., Machida, M., Shigeyoshi, Y., Iino, M., and Hashimoto, S. (2005). System-level identification of transcriptional circuits underlying mammalian circadian clocks. Nat. Genet. 37, 187–192.

Ukai-Tadenuma, M., Kasukawa, T., and Ueda, H.R. (2008). Proof-by-synthesis of the transcriptional logic of mammalian circadian clocks. Nat. Cell Biol. 10, 1154–1163.

Ukai, H., Kobayashi, T.J., Nagano, M., Masumoto, K.H., Sujino, M., Kondo, T., Yagita, K., Shigeyoshi, Y., and Ueda, H.R. (2007). Melanopsin-dependent photo-perturbation reveals desynchronization underlying the singularity of mammalian circadian clocks. Nat. Cell Biol. 9, 1327–1334.

van der Horst, G.T., Muijtjens, M., Kobayashi, K., Takano, R., Kanno, S., Takao, M., de Wit, J., Verkerk, A., Eker, A.P., van Leenen, D., et al. (1999). Mammalian Cry1 and Cry2 are essential for maintenance of circadian rhythms. Nature 398, 627–630.

Yoo, S.H., Ko, C.H., Lowrey, P.L., Buhr, E.D., Song, E.J., Chang, S., Yoo, O.J., Yamazaki, S., Lee, C., and Takahashi, J.S. (2005). A noncanonical E box enhancer drives mouse Period2 circadian oscillations in vivo. Proc. Natl. Acad. Sci. USA 102, 2608–2613.

Young, M.W., and Kay, S.A. (2001). Time zones: a comparative genetics of circadian clocks. Nat. Rev. Genet. 2, 702–715.

Supplemental Information

EXTENDED EXPERIMENTAL PROCEDURES

Real-Time Circadian Reporter Assay Using NIH 3T3 Cells

Real-time circadian assays were performed as previously described (Sato et al., 2006; Ueda et al., 2005) with the following modifications. NIH 3T3 cells (American Type Culture Collection) were grown in DMEM (Invitrogen) supplemented with 10% FBS (JRH Biosciences) and antibiotics (100 U/ml penicillin and 100 µg/ml streptomycin, Invitrogen). Cells were plated at 1×10^5 cells per well in 35-mm dishes 24 hr before transfection. These cells were transfected with FuGene6 (Roche) according to the manufacturer's instructions. The cells in each well were transfected with 0.4 µg of the each *Luciferase* reporter plasmids. The amount of transfected plasmid was adjusted to 2.0 µg with empty vector. After 72 hr, the media in each well was replaced with 2 ml of culture medium (DMEM/10% FBS) supplemented with 10 mM HEPES (pH 7.2, Invitrogen), 0.1 mM luciferin (Promega), antibiotics, and 10 µM forskolin (Fermentek). Bioluminescence was measured with photomultiplier tube detector assemblies (LM2400R, Hamamatsu Photonics). The modules and cultures were maintained in a darkroom at 30°C and interfaced with computers for continuous data acquisition. Photons were counted for 1 min at 12 min intervals.

Transfection and Luciferase Assay

NIH 3T3 cells (American Type Culture Collection) were maintained in DMEM (Invitrogen) supplemented with 10% FBS (JRH Biosciences) and antibiotics (100 U/ml penicillin and 100 µg/ml streptomycin; Invitrogen). One day prior to transfection, cells were plated onto six-well plates at a density of 2×10^5 cells per well. The following day, cells were co-transfected using FuGene6 (Roche) with 0.4 µg of a *Luciferase* reporter plasmid in the presence of the following constructs as indicated in respective figures: 0 or 0.4 µg each of pMU2-*Bmal1* (Kumaki et al., 2008) and pMU2-*Clock* (Kumaki et al., 2008), and 0, 0.8, 1.6 or 3.2 µg of pMU2-*E4bp4* (Kumaki et al., 2008) (for Figure 1F); 0 or 0.4 µg each of pMU2-*Bmal1* and pMU2-*Clock*, and 0 or 1.6 µg of pMU2-*Cry1* (For **Figure S1C**); 0 or 0.8 µg of pMU2-*Dbp* (Kumaki et al., 2008), pMU2-*Tef*, pMU2-*Hlf* (for Figure S1D); and 0 or 0.4 µg of pMU2-*Rorα* (Kumaki et al., 2008) (for Figure 3B). Empty vector was used to make up the total amount of DNA to 4.0 µg per well. Additionally, 50 ng of a phRL-SV40 plasmid (Renilla *luciferase* (*RLuc*) reporter vector, Promega) was added into each transfection as an internal control for transfection efficiency. Forty-eight hours after transfection, cells were harvested and assayed with Dual-Luciferase Reporter Assay System (Promega). Luciferase activity was normalized by *Rluc* activity.

mRNA Expression Measurement of Endogenous *Cry1*, *Per2*, and *Bmal1* and Exogenous Luciferase by Quantitative PCR

Temporal mRNA profiles of endogenous *Per2*, *Bmal1*, and *Cry1* in transfected NIH 3T3 reporter cells expressing a P(*Cry1*)-*Luc* or a P(*Per2*)-*Luc* reporter were measured by quantitative PCR. We sampled the transfected NIH 3T3 cells every 4 hr over 3 days after synchronizing cells by forskolin stimulation.

NIH 3T3 cells were grown in DMEM (Invitrogen) supplemented with 10% FBS (JRH Biosciences) and antibiotics (100 U/ml penicillin and 100 µg/ml streptomycin; Invitrogen). NIH 3T3 cells were plated at a density of 9×10^5 cells per well in 12 of 90-mm dishes. The following day, NIH 3T3 cells were transfected using FuGene6 (Roche) with 5.4 µg of pMU2-P(*Per2*)-*Luc* or pMU2-P(*Cry1*)-*Luc* plasmid according to the manufacturer's instructions. Empty vector was used to make up the total amount of DNA to 18.0 µg per dish. After 24 hr, cells in each dish were harvested and plated in 76 of 35-mm dishes. After 48 hr, medium in each dish was replaced with 2 ml of culture medium (DMEM/10% FBS) supplemented with 10 mM HEPES (pH 7.2, Invitrogen), 0.1 mM luciferin (Promega), antibiotics, and 10 µM forskolin (Fermentek), and subsequently cultured at 30°C. Cells were sampled every 4 hr for 3 days (n = 3 dishes). Total RNA was prepared from 35-mm dishes at each time point using TRIzol reagents (Invitrogen), and purified with RNeasy kit (QIAGEN) and RNase-free DNase set (QIAGEN) according to the manufacturer's instructions. The cDNA was synthesized from 0.25 µg of total RNA with random 6-mer (Promega) and Superscript II Reverse Transcriptase (Invitrogen) according to the manufacturer's instructions. Quantitative PCR (qPCR) was performed using ABI Prism 7700 and Power SYBR Green Reagents (Applied Biosystems). Samples contained $1 \times$ Power SYBR Green Master Mix (Applied Biosystems), 0.5 µM primers and 1/20 synthesized cDNA in a 10 µl volume. PCR conditions were as follows: 10 min at 95°C, then 45 cycles of 15 s at 94°C, 30 s at 59°C and 1 min at 72°C. Absolute cDNA abundance was calculated using a standard curve obtained from genomic DNA and pMU2-*Luc* plasmid DNA. *Gapdh* expression levels were quantified and used as an internal control.

The expression phases were obtained from analyses of temporal mRNA profiles by fitting a cosine wave of 21.5 hr period, as estimated from circadian bioluminescence rhythms monitored in parallel.

Primer Sequences Used in Quantitative PCR

Cry1 *3′-UTR*
Forward primer, 5′-TGAGGCAAGCAGACTGAATATTG-3′; reverse, 5′-CCTCTGTACCGGGAAAGCTG-3′.
Per2 *3′-UTR*
Forward primer, 5′-TGTGCGATGATGATTCGTGA-3′; reverse, 5′-GGTGAAGGTACGTTTGGTTTGC-3′.
Bmal1 *3′-UTR*
Forward primer, 5′-CCACCTCAGAGCCATTGATACA-3′; reverse, 5′-GAGCAGGTTTAGTTCCACTTTGTCT-3′.
Gapdh

Forward primer, 5′-CAAGGAGTAAGAAACCCTGGACC-3′; reverse, 5′-CGAGTTGGGATAGGGCCTCT-3′.
Luciferase
Forward primer, 5′-CTTACTGGGACGAAGACGAACAC-3′; reverse, 5′-GAGACTTCAGGCGGTCAACG-3′.

Chromatin Immunoprecipitation from Mouse Liver Chromatin

Chromatin samples from mouse liver were obtained from $Dbp^{-/-}$ mice (Lopez-Molina et al., 1997) (kind gift from U. Schibler, Geneva) or $Rev\text{-}Erb\alpha^{-/-}$ mice (Preitner et al., 2002) (kind gift from U. Albrecht, Fribourg). In brief, mouse liver was homogenized in 1 × PBS supplemented with 1% formaldehyde (Ripperger and Schibler, 2006). Following 5 min incubation at RT, the reaction was quenched by addition of three volume of ice-cold 2.4 M sucrose, 10 mM HEPES pH 7.6, 15 mM KCl, 0.5 mM spermidine, 0.15 mM spermine, 150 mM glycine, 1 mM DTT. The sample was layered on top of a 2.05 M sucrose/ 10% glycerol cushion in the same buffer, and centrifuged for 1 hr at 4°C and 100,000 × g. The pellet containing purified nuclei was resuspended in 1% SDS, 20 mM Tris-HCl pH 7.4, 150 mM NaCl, 2 mM EDTA, and sonicated five times using a micro-tip device for the ultrasonic homogenizer 300V/T (BioLogics). The dilution conditions, the pre-clearing step, the co-immunoprecipitation conditions, the washing conditions, the reversal of the cross-links and the subsequent purification of the DNA fragments, and the antibodies (anti-BMAL1, anti-DBP and anti-REV-ERBα) used have been described (Schmutz et al., 2010; Wuarin and Schibler, 1990). The co-immunoprecipitated DNA-fragments were quantified using TaqMan RT-PCR using a RotorGene 6200 RT-PCR machine (Corbett Life Science) and EX Taq PCR master mix (TaKaRa Bio, Inc.). Specific TaqMan probes were used to detect the *Cry1* promoter region, the *Cry1* 1st intron region, or the *Dbp* promoter region (control region).

Probe Sequences Used in Quantitative PCR

FAM, 6-carboxyfluorescin; TAMRA, 6-carboxytetramethylrhodamine; BHQ1, black hole quencher1.
Dbp *Promoter (Control Region)*
Forward, 5′-ACACCCGCATCCGGTAGC-3′; reverse, 5′-CCACTTCGGGCCAATGAG-3′; probe, 5′-FAM-CGCGCAAAGCCATGTG CTTCC-TAMRA-3′.
Cry1 *Promoter*
Forward, 5′-CGCAACCGGTCCCGAAGCA-3′; reverse, 5′-ACCACCGGCACCTCACGTTT-3′; probe, 5′-FAM-TCAGACCCCCGCG TGCGCCG-BHQ1-3′.
Cry1 *1st intron*
Forward, 5′-TCATTGTGATGGGAGTATGC-3′; reverse, 5′-TCCAAAAGATGATTTCAACA-3′; probe, 5′-FAM-CACCCACTGGTTG CTATAGCGA-BHQ1-3′.

Quantitative PCR from Mouse Liver RNA

RNA samples from mouse liver were obtained from PAR bZip triple knockout mice ($Dbp^{-/-}$:$Tef^{-/-}$:$Hlf^{-/-}$) (Gachon et al., 2004) and wild-type mice (kind gift from F. Gachon, Lausanne). In brief, total RNA was extracted from liver tissue using RNA-Bee (AMS Biotechnology) according to the manufacturer's instructions. ssDNA complementary to the RNA starting from hybridized random hexamer primers was synthesized with SuperScript II (Life Technology Corporation) according to the manufacturer's instructions. The products were quantified using TaqMan RT-PCR using a RotorGene 6200 RT-PCR machine (Corbett Life Science) and EX Taq PCR master mix (TaKaRa Bio, Inc.). All RNA samples were normalized to *Gapdh* mRNA accumulation.

Probe Sequences Used in Quantitative PCR

FAM, 6-carboxyfluorescin; TAMRA, 6-carboxytetramethylrhodamine; MGB, minor groove binder.
Cry1
Forward, 5′-CTGGCGTGGAAGTCATCGT-3′; reverse, 5′-CTGTCCGCCATTGAGTTCTATG-3′; probe, 5′-FAM-CGCATTTCACATA CACTGTATGACCTGGACA-TAMRA-3′.
Bmal1
Forward, 5′-CCAAGAAAGTATGGACACAGACAAA-3′; reverse, 5′-GCATTCTTGATCCTTCCTTGGT-3′; probe, 5′-FAM-TGACCC TCATGGAAGGTTAGAATATGCAGAA-TAMRA-3′.
Rev-Erbα
Forward, 5′-CATGGTGCTACTGTGTAAGGTGTGT-3′; reverse, 5′-CACAGGCGTGCACTCCATAG-3′; probe, 5′-FAM-ACGTGGCC TCAGGC-MGB-3′.
Per1
Forward, 5′-ACCAGCGTGTCATGATGACATAC-3′; reverse, 5′-CTCTCCCGGTCTTGCTTCAG-3′; probe, 5′-FAM-CCGTCCAGGG ATGCAGCCTCTG-TAMRA-3′.
Dbp
Forward, 5′-CGTGGAGGTGCTTAATGACCTTT-3′; reverse, 5′-CATGGCCTGGAATGCTTGA-3′; probe, 5′-FAM-AACCTGATCCCG CTGATCTCGCC-TAMRA-3′.
Tef

Forward, 5′-GCCGAGCTTCGCAAGGA-3′; reverse, 5′-ACAGGTTACAAGGGCCCGTACT-3′; probe, 5′-FAM-ACACGATGGTCTT GCACTTGCCCA-TAMRA-3′.

Hlf

Forward, 5′-AGGCGCAGAAAGAACAACATG-3′; reverse, 5′-GAATGAGGCCCGGATTGC-3′; probe, 5′-FAM-CGGCCAAGCGCT CCCGTG-TAMRA-3′.

Gapdh

Forward, 5′-CATGGCCTTCCGTGTTCCTA-3′; reverse: 5′-CCTGCTTCACCACCTTCTTGA-3′; probe, 5′-FAM-CCGCCTGGAGAAA CCTGCCAAGTATG-TAMRA-3′.

Preparation of Embryonic Fibroblasts from $Cry1^{-/-}$:$Cry2^{-/-}$ Double-Knockout Mice

$Cry1^{-/-}$:$Cry2^{-/-}$ double knockout mice (van der Horst et al., 1999) were carefully kept and handled according to the RIKEN Regulations for Animal Experiments. Embryos of $Cry1^{-/-}$:$Cry2^{-/-}$ double knockout mice at E13-14 were excised and washed several times with Hanks' balanced salt solution. After the placenta and internal organs were completely removed, the embryos were cut into small pieces, and the cells were dissociated by incubation in 0.05% trypsin solution with 0.53 mM EDTA for 30 min at 37°C. The dissociated cells (mouse embryonic fibroblasts (MEF) from $Cry1^{-/-}$:$Cry2^{-/-}$ double knockout mice; $Cry1^{-/-}$:$Cry2^{-/-}$ cells) were suspended and cultured in DMEM (Invitrogen) supplemented with 10% FBS (JRH Biosciences) and antibiotics (100 U/ml penicillin and 100 μg/ml streptomycin, Invitrogen).

Real-Time Circadian Reporter Assay Using $Cry1^{-/-}$:$Cry2^{-/-}$ Cells

Real-time circadian assays were performed as described above with the following modifications. $Cry1^{-/-}$:$Cry2^{-/-}$ cells were plated at 4×10^5 cells per well in 35-mm dishes 24 hr before transfection. The cells in each well were transfected with FuGene6 with 3.95 μg of pGL3-P($Per2$)-dLuc reporter plasmid (Sato et al., 2006) and 0.15 μg of each $Cry1$ gene expression vector. The amount of transfected plasmid was adjusted to 4.1 μg with empty vector. After 72 hr, the medium in each well was replaced with 2 ml of culture medium (DMEM/10% FBS) supplemented with 10 mM HEPES (pH 7.2), 0.1 mM luciferin, antibiotics, and 30 μM forskolin (Fermentek). Bioluminescence was measured with photomultiplier tube detector assemblies (LM2400R, Hamamatsu Photonics) at 30°C.

Real-Time Circadian Reporter Assay and Measurement of Rluc Activity Using $Rluc$ Fused $Cry1$

Real-time circadian assays were performed as described above with the following modifications. $Cry1^{-/-}$:$Cry2^{-/-}$ cells were plated at 4×10^5 cells per well in two 35-mm dishes 24 hr before transfection. The cells in each two well were transfected with FuGene6 (Roche) with 3.95 μg of pGL3-P($Per2$)-dLuc reporter plasmid (Sato et al., 2006) in the presence of the following constructs as indicated in respective figures: 1.5, 0.45 or 0.15 μg (for Figure S5A) and 0.3, 0.2 or 0.15 μg (for Figure S6E) of each $Cry1$-$Rluc$ fusion gene expression vector. The amount of transfected plasmid was adjusted to 5.5 μg with empty vector. After 24 hr, the cells in each two well were harvested and plated in two 35-mm dishes. After 48 hr, bioluminescence was measured with photomultiplier tube detector assemblies (LM2400R, Hamamatsu Photonics) at 30°C with the cells in each one 35-mm dishes, which was replaced with 2 ml of culture medium (DMEM/10% FBS) supplemented with 10 mM HEPES (pH 7.2), 0.1 mM luciferin, antibiotics, and 30 μM forskolin (Fermentek). In the same time, cells in each another well were harvested and measured Rluc activity with Dual-Luciferase Reporter Assay System (Promega). To measure the average of CRY1 protein levels over a circadian period, the timing of measurement was just before the stimulation where the population of cells had a mixture of different circadian phases.

Real-Time Single-Cell Bioluminescence Imaging

$Cry1^{-/-}$:$Cry2^{-/-}$ cell samples were prepared as described above with the following modifications. Six-well culture plate was sealed with coverslips, placed on the stage of a luminescence microscope (Luminoview LV100, Olympus), and kept at 30°C in a heated chamber (Olympus). Bioluminescence was imaged using a 10 × objective (10 × /0.40 U Plan SApo, Olympus) and transmitted to a cooled CCD camera (ORCA-II ER, Hamamatsu Photonics) mounted on the bottom port of the microscope. Readout noise was reduced by using 2 × 2 binning of the 672 × 512 pixel array. Four samples were measured at the same experiment. Time-lapse images were collected at 120 min intervals with 28 min exposures per sample by a computer using image analysis software (Metamorph, Molecular Devices).

Image Processing of Real-Time Single-Cell Bioluminescence Images

Hot pixels and cosmic rays were removed by applying spatial and temporal local median filters, respectively using Matlab (Math-Works). The position of a hot pixel was detected by comparing the time-variation of the pixel with surrounding pixels. The cosmic rays were detected by comparing the intensities of pixels for the temporally adjacent images. The bioluminescence of each cell was estimated by averaging pixels within the region of interest manually defined for each cell by a custom-made software program developed with Matlab. Remaining data processing of the obtained single-cell bioluminescence data was conducted using Mathematica (Wolfram Research).

Construction of Plasmids
pMU2-P(Cry1)-Luc
The coding sequence of *Luciferase* (*Luc*) was amplified from pGL3 plasmid (Promega) using PCR with the following primers: Forward primers containing *PI-Psp*I recognition sequence: (5′-*TGGCAAACAGCTATTATGGGTATTAT GGGT*GAAGACGCCAAAAAC ATAAAG-3′, recognition sequence is indicated with italics, Hokkaido System Science), Reverse primers containing *PI-Sce*I recognition sequence: (5′-*TGCCATTTCATTACCTCTTTCTCCGCACCCGACATAGA T*TTACACGGCGATCTTTCCGC-3′). PCR product was digested with *PI-Psp*I and *PI-Sce*I (New England BioLabs) and cloned into pMU2-MCS vector (Ukai et al., 2007), and the resulting vector was designated as pMU2-MCS-*Luc*.

A 1.5 kb promoter region of mouse *Cry1* gene was amplified from NIH 3T3 genomic DNA using PCR with forward primers containing *Mlu*I recognition sequence (5′-*ACGC GT*GTAAAGATGCACATGTGGCCCTG-3′, recognition sequence is indicated with italics, Hokkaido System Science) and reverse primers containing BglII recognition sequence (5′-*AGATCT*CGTCCGGAG GACACGCA TACC-3′). PCR product of 1.5 kb *Cry1* promoter fragment was digested with *Mlu*I and BglII. The promoter fragment was cloned into the *Mlu*I-BglII site of pMU2-MCS-*Luc* vector immediately upstream of *Luc* to obtain pMU2-P(*Cry1*)-*Luc*.

pMU2-3 × E′ Box-P(SV40)-Luc, pMU2-3 × D Box-P(SV40)-Luc, pMU2-3 × RRE- P(SV40)-Luc, pMU2-P(SV40)-Luc
pGL3-3 × CCE-P(SV40)-d*Luc* plasmids (Ueda et al., 2005; Ukai-Tadenuma et al., 2008) contain one of the clock-controlled elements (or CCEs; italicized): *Per2* E′ box (5′-GCGCGCGCGGT*CACGTT*TTCCACTATGTG ACAGCGGAGG-3′), *Per3* D box (5′-CCCGCGCG*TTATGTAA*GGTACTCG-3′) or *Bmal1* RRE (5′-AGGCAG*AAAGTAGGTCA*GGGACG-3′). pGL3-P(SV40)-d*Luc* is a parental plasmid. These vectors were digested with KpnI and HindIII, and the obtained 3 × E' box-P(SV40), 3 × D box-P(SV40), 3 × RRE-P(SV40), and P(SV40) promoter fragments were cloned into the KpnI-*Hind*III sites in a pMU2-MCS-*Luc* vector upstream of *Luc*, and the resulting vectors were designated as pMU2-3 × E' box-P(SV40)-*Luc*, pMU2- 3 × D box-P(SV40)-*Luc*, pMU2-3 × RRE-P(SV40)-*Luc* and pMU2-P(SV40)-*Luc*, respectively.

pMU2-3 × Cry1proD-P(SV40)-Luc and pMU2-3 × Cry1proD mutant-P(SV40)-Luc
Oligonucleotides (Hokkaido System Science) containing three tandem repeats of wild-type or mutated Cry1proD elements were annealed and inserted into the *Mlu*I-BglII sites upstream of pMU2-P(SV40)-*Luc* (see above), and the resulting vectors were designated as pMU2-3 × Cry1proD-P(SV40)-*Luc* and pMU2-3 × Cry1proD mutant- P(SV40)-*Luc*.

Oligonucleotide Sequences for Three Tandem Repeats of Cry1proD Element
Cry1proD Wild-Type
Forward oligonucleotide, 5′-CGCGAAACACACTTCAGAAACGTGAGGTAAACACACTTCAGAAACGTGAGGTAAACACACTTCAG AAACGTGAGGT-3′; reverse, 5′-GATCACCTCACGTTTCTGAAGTGTGTTTACCTCACGTTTCTGAAGTGTGTTTACCTCACGTTTCTG AAGTGTGTTT-3′.

Cry1proD Mutant
Forward oligonucleotide, 5′-CGCGAAACACACCACCCGGCCGTGAGGTAAACACACCACCCGGCCGTGAGGTAAACACACCAC CCGGCCGTGAGGT-3′; reverse, 5′-GATCACCTCACGGCCGGGTGGTGTGTTTACCTCACGGCCGGGTGGTGTGTTTACCTCACGG CCGGGTGGTGTGTTT-3′.

pMU2-Cry1
The full-length coding sequence of mouse *Cry1* was amplified from pCI-*Cry1* by PCR using forward primers containing *I-Sce*I recognition sequence (5′-*ATTACCCTGTTATCCCTA*ATGGGGTGAACGCCGTGCAC-3′, recognition sequence is indicated with italics, Hokkaido System Science) and reverse primers containing *PI-Psp*I recognition sequence (5′-*ACCCATAATACCCATAA TAGCTGTTT GCCA*GTTACTGCTCTGCCGCTGG-3′). PCR product was digested with *I-Sce*I and *PI-Psp*I (New England BioLabs) and cloned into pMU2 vector (Ukai et al., 2007), and the resulting construct was designated as pMU2-*Cry1*. In this pMU2 vector, *Cry1* gene is regulated by a CMV promoter.

pMU2-Hlf and pMU2-Tef
The full-length coding sequences of mouse *Hlf* and *Tef* were amplified from NIH 3T3 cDNA library by PCR using forward primers containing *I-Sce*I recognition sequence and reverse primers containing *PI-Psp*I recognition sequence (Hokkaido System Science). PCR product was digested with *I-Sce*I and *PI-Psp*I (New England BioLabs) and cloned into pMU2 vector (Ukai et al., 2007), and the resulting vectors were designated as pMU2-*Hlf* and pMU2-*Tef*. In these pMU2 vectors, genes are regulated by a CMV promoter.

Oligonucleotide Sequences for Cloning of Hlf and Tef
Cloning of Hlf
Forward primer, 5′-*ATTACCCTGTTATCCCTA*ATGAGAAAATGTCCCGACAGCTCC-3′; reverse, 5′-*ACCCATAATACCCATAATAG CTGTTTGCCA*CAGGGGCCCGTGCCTGGCCTC-3′.

Cloning of Tef
Forward primer, 5′-*ATTACCCTGTTATCCCTA*ATGACATGCCTGAGGTCCTCAAGTCC-3′; reverse, 5′-*ACCCATAATACCCATAATAGCTGTTTGCCA*CAAGGGCCCGTACTTGGTCTCG-3′.

pMU2-P(Per2)-Luc
Per2 promoter was digested from pGL3-P(*Per2*) (Sato et al., 2006) with *Mlu*I and BglII. Promoter fragments were cloned into the *Mlu*I-BglII sites of pMU2-MCS-*Luc* vector upstream of *Luc* and designated as pMU2-P(*Per2*)-*Luc*.

pMU2-P(Cry1)-Cry1 Intron 1.03k-Luc, pMU2-P(Cry1)-Cry1 Intron 336-Luc, and pMU2-P(Cry1)-Cry1 Intron ∆336-Luc

We amplified the 1.03 kb and 336 base intron regions of mouse *Cry1* from NIH 3T3 genomic DNA by PCR with forward and reverse primers containing *I-Sce*I recognition sequence (Hokkaido System Science). PCR products were cloned into pCR2.1-TOPO (Invitrogen) and designated as pCR2.1-*Cry1* intron 1.03k and pCR2.1-*Cry1* intron 336. We used inverse PCR to modify the *Cry1* intron sequence. For construction of pCR2.1-*Cry1* intron ∆336, we used pCR2.1-*Cry1* intron 1.03k as a template. Inverse PCR products were treated with Mighty Cloning kit (TaKaRa) for 5′-end phosphorylation, and subsequently self-ligated. These constructs were digested with *I-Sce*I, and pMU2-P(*Cry1*)-*Luc* plasmid (see above) was also digested with *I-Sce*I. The three *Cry1* intron fragments were ligated at the *I-Sce*I site of pMU2-P(*Cry1*)-*Luc*, and designated as pMU2-P(*Cry1*)-*Cry1* intron 1.03k-*Luc*, pMU2-P(*Cry1*)-*Cry1* intron 336-*Luc* and pMU2-P(*Cry1*)-*Cry1* intron ∆336 -*Luc*, respectively.

Oligonucleotide Sequences for Construction of Cry1 Introns
Cloning of Cry1 Intron Sequence (1.03 kb)
Forward primer, 5′-*ATTACCCTGTTATCCCTA*ATCGAGATGGTTAAGTCGGGTCTCTAGGGTC-3′; reverse, 5′-*TAGGGATAACAGG GTAAT*CTTGACAGCTCAGGATCGCACTAAACGTGTG-3′.
Cloning of Cry1 Intron 336 Sequence
Forward primer, 5′-*ATTACCCTGTTATCCCTA*ATCGAGATGGTTGTTATGACACAGTGTAGAAAC-3′; reverse, 5′-*TAGGGATAACA GGGTAAT*CTTGACAGCTCTACCTTTTACTACTATAAAAACGTAC-3′.
Inverse PCR of Cry1 Intron ∆336
Forward primer, 5′-AATTCTCGAGATAACAGTCACCAGTGGAG-3′; reverse, 5′-AATTCTCGAGAGGTAGTGATTTCTAGAGG-3′.
pMU2-Cry1 Intron 336-P(Cry1)-Luc, pMU2-P(Cry1)-Cry1 Intron 336-Flag-Luc, and pMU2-P(Cry1)-Luc-Cry1 Intron 336
pMU2-P(*Cry1*)-*Luc* plasmid was digested with KpnI (upstream of *Cry1* promoter), *I-Ceu*I (downstream of *Cry1* promoter, New England BioLabs) or *PI-Sce*I (downstream of coding sequence, New England BioLabs), and then blunted with T4 DNA polymerase. pCR2.1-*Cry1* intron 336 (see above) was digested with *I-Sce*I, and blunted with T4 DNA polymerase. The *Cry1* intron 336 fragment was ligated at KpnI, *I-Ceu*I or *PI-Sce*I site of pMU2-P(*Cry1*)-*Luc*, and designated as pMU2-*Cry1* intron 336-P(*Cry1*)-*Luc*, pMU2-P (*Cry1*)-*Cry1* intron 336-Flag-*Luc*, pMU2-P(*Cry1*)-*Luc*-*Cry1* intron 336, respectively.
pMU2-P(SV40)-Cry1 Intron 336-Luc, pMU2-P(SV40)-Cry1 Intron 336 R1 Deletion- Luc, pMU2-P(SV40)-Cry1 Intron 336 R2 Deletion-Luc, pMU2-P(SV40)-Cry1 Intron 336 R1,2 Deletion-Luc, pMU2-P(SV40)-Cry1 Intron 336 R1 Mutation-Luc, pMU2- P(SV40)-Cry1 Intron 336 R2 Mutation-Luc, pMU2-P(SV40)-Cry1 Intron 336 R1,2 Mutation-Luc, pMU2-P(SV40)- Cry1 Intron 336 R1 Inversion-Luc, pMU2-P(SV40)- Cry1 Intron 336 R2 Inversion-Luc, and pMU2-P(SV40)-Cry1 Intron 336 R1,2 Inversion-Luc

First, we constructed various modified *Cry1* intron 336. For construction of pCR2.1-*Cry1* intron 336 R1 deletion, pCR2.1-*Cry1* intron 336 R2 deletion, pCR2.1-*Cry1* intron 336 R1,2 deletion, pCR2.1-*Cry1* intron 336 R1 mutation, pCR2.1-*Cry1* intron 336 R2 mutation, pCR2.1-*Cry1* intron 336 R1,2 mutation, pCR2.1-*Cry1* intron 336 R1 inversion, pCR2.1-*Cry1* intron 336 R2 inversion, and pCR2.1-*Cry1* intron 336 R1,2 inversion, we used pCR2.1-*Cry1* intron 336 (see above) as a template. Inverse PCR products were treated with Mighty Cloning kit (TaKaRa) for 5′-end phosphorylation, and subsequently self-ligated. These constructs and pMU2-P(SV40)-*Luc* (see above) plasmids were digested with *I-Sce*I. The altered *Cry1* intron fragments were ligated at the *I-Sce*I site of pMU2-P(SV40)-*Luc*, and designated as pMU2-P(SV40)-*Cry1* intron 336-*Luc*, pMU2-P(SV40)-*Cry1* intron 336 R1 deletion- *Luc*, pMU2-P(SV40)-*Cry1* intron 336 R2 deletion-*Luc*, pMU2-P(SV40)-*Cry1* intron 336 R1,2 deletion-*Luc*, pMU2-P(SV40)-*Cry1* intron 336 R1 mutation-*Luc*, pMU2- P(SV40*1*)-*Cry1* intron 336 R2 mutation-*Luc*, pMU2-P(SV40)-*Cry1* intron 336 R1,2 mutation-*Luc*, pMU2-P(SV40)-*Cry1* intron 336 R1 inversion-*Luc*, pMU2-P(SV40)- *Cry1* intron 336 R2 inversion-*Luc*, and pMU2-P(SV40)-*Cry1* intron 336 R1,2 inversion-*Luc*, respectively.

Primer Sequence for the Inverse PCR
Cry1 Intron 336 R1 Deletion
Forward primer, 5′-GGTCATTGTGATGGGAGTATGC-3′; reverse, 5′-CTAGTCTGTGCTAGGACAGC-3′.
Cry1 Intron 336 R2 Deletion
Forward primer, 5′-GAAACTATTTCTGTTGATTCATGTTG-3′; reverse, 5′-GGTCATCGCTATAGCAACCAG-3′.
Cry1 Intron 336 R1,2 Deletion
Forward primer, 5′-GAAACTATTTCTGTTGATTCATGTTG-3′; reverse, 5′-CTAGTCTGTGCTAGGACAGC-3′.
Cry1 Intron 336 R1 Mutation
Forward primer, 5′-AAAGTCCTAGCTTGTGATGGGAGTATGCTAAAC-3′; reverse, 5′-CTAGTCTGTGCTAGGACAGC-3′.
Cry1 Intron 336 R2 Mutation
Forward primer, 5′-GAAACTATTTCTGTTGATTCATGTTG-3′; reverse, 5′-TAAAGTCCTAGCTCGCTATAGCAACCAGTG-3′.
Cry1 Intron 336 R1 Inversion
Forward primer, 5′-TGACCTACTTTTTGTGATGGGAGTATGCTAAAC-3′; reverse, 5′-CTAGTCTGTGCTAGGACAGC-3′.
Cry1 Intron 336 R2 Inversion
Forward primer, 5′-GAAACTATTTCTGTTGATTCATGTTG-3′; reverse, 5′-TTGACCTACTTTTCGCTATAGCAACCAGTG-3′.

pMU2-P(Cry1)-Cry1 Intron 336 R1 Deletion-Luc, pMU2-P(Cry1)-Cry1 Intron 336 R2 Deletion-Luc, pMU2-P(Cry1)-Cry1 Intron 336 R1,2 Deletion-Luc, pMU2- P(Cry1)-Cry1 Intron 336 R1 Mutation-Luc, pMU2-P(Cry1)-Cry1 Intron 336 R2 Mutation-Luc, pMU2-P(Cry1)-Cry1 Intron 336 R1,2 Mutation-Luc, pMU2-P(Cry1)-Cry1 Intron 336 R1 Inversion-Luc, pMU2-P(Cry1)-Cry1 Intron 336 R2 Inversion-Luc, and pMU2-P(Cry1)-Cry1 Intron 336 R1,2 Inversion-Luc

First, the following vectors were digested with *I-Sce*I: pCR2.1-*Cry1* intron 336 R1 deletion, pCR2.1-*Cry1* intron 336 R2 deletion, pCR2.1-*Cry1* intron 336 R1,2 deletion, pCR2.1- *Cry1* intron 336 R1 mutation, pCR2.1-*Cry1* intron 336 R2 mutation, pCR2.1-*Cry1* intron 336 R1,2 mutation, pCR2.1-*Cry1* intron 336 R1 inversion, pCR2.1-*Cry1* intron 336 R2 inversion, and pCR2.1-*Cry1* intron 336 R1,2 inversion (see above), and pMU2-P(*Cry1*)-*Luc* plasmid (see above). The altered *Cry1* intron fragments were ligated at the *I-Sce*I site of pMU2-P(*Cry1*)-*Luc*, and designated as pMU2-P(*Cry1*)-*Cry1* intron 336 R1 deletion- *Luc*, pMU2-P(*Cry1*)-*Cry1* intron 336 R2 deletion-*Luc*, pMU2-P(*Cry1*)-*Cry1* intron 336 R1,2 deletion-*Luc*, pMU2-P(*Cry1*)-*Cry1* intron 336 R1 mutation-*Luc*, pMU2-P (*Cry1*)- *Cry1* intron 336 R2 mutation-*Luc*, pMU2-P(*Cry1*)-*Cry1* intron 336 R1,2 mutation-*Luc*, pMU2-P(*Cry1*)-*Cry1* intron 336 R1 inversion-*Luc*, pMU2-P(*Cry1*)-*Cry1* intron 336 R2 inversion-*Luc*, and pMU2-P(*Cry1*)-*Cry1* intron 336 R1,2 inversion-*Luc*, respectively.

pMU2-3 × E′ Box-P(SV40)-Cry1 Intron 336-Luc, pMU2-3 × D Box-P(SV40)-Cry1 Intron 336-Luc, and pMU2-3 × RRE-P(SV40)-Cry1 Intron 336-Luc

pCR2.1-*Cry1* intron 336 (see above) was digested with *I-Sce*I. pMU2-3 × E' box-P(SV40)-*Luc*, pMU2-3 × D box-P(SV40)-*Luc*, and pMU2-3 × RRE-P(SV40)-*Luc* plasmids (see above) were also digested with *I-Sce*I. The *Cry1* intron 336 fragment was ligated at the *I-Sce*I site of these plasmids, and designated as pMU2-3 × E' box-P(SV40)-*Cry1* intron 336- *Luc*, pMU2-3 × D box-P(SV40)-*Cry1* intron 336-*Luc*, and pMU2-3 × RRE-P(SV40)-*Cry1* intron 336-*Luc*, respectively.

pMU2-P(Cry1)-Cry1

We amplified the full-length coding sequence of mouse *Cry1* from pCI-*Cry1* by PCR with forward primers containing *PI-Psp*I recognition sequence (5′-*TGGCAAACAGCTATTATGGGTATTATGGGT*GGGGTGAACGCCGTGCAC-3′, recognition sequence is indicated with italics, Hokkaido System Science) and reverse primers containing *PI-Sce*I recognition sequence (5′-*TGCCATTTCATTACCTCTTTCTCCGCACCCGACATAGAT*TCAGTTACTGCTCTGCCGCTGG-3′). PCR product was digested with *PI-Psp*I and *PI-Sce*I (New England BioLabs) and cloned into pMU2-P(*Cry1*)-*Luc* vector (see above) in replace of the *Luc* gene, and the resulting vector was designated as pMU2-P(*Cry1*)-*Cry1*.

pMU2-P(Cry1)-Cry1 Intron 336-Cry1, pMU2-P(Cry1)-Cry1 Intron 336 R1 Deletion-Cry1, pMU2-P(Cry1)-Cry1 Intron 336 R2 Deletion-Cry1, pMU2-P(Cry1)-Cry1 Intron 336 R1,2 Deletion-Cry1, pMU2-P(Cry1)-Cry1 Intron 336 R1 Mutation-Cry1, pMU2-P(Cry1)-Cry1 Intron 336 R2 Mutation-Cry1, pMU2-P(Cry1)-Cry1 Intron 336 R1,2 Mutation-Cry1, pMU2-P (Cry1)-Cry1 Intron 336 R1 Inversion-Cry1, pMU2- P(Cry1)-Cry1 Intron 336 R2 Inversion-Cry1, and pMU2-P(Cry1)Cry1 Intron 336 R1,2 Inversion-Cry1

The following vectors were first digested with *I-Sce*I: pCR2.1-*Cry1* intron 336, pCR2.1-*Cry1* intron 336 R1 deletion, pCR2.1-*Cry1* intron 336 R2 deletion, pCR2.1-*Cry1* intron 336 R1,2 deletion, pCR2.1-*Cry1* intron 336 R1 mutation, pCR2.1-*Cry1* intron 336 R2 mutation, pCR2.1-*Cry1* intron 336 R1,2 mutation, pCR2.1-*Cry1* intron 336 R1 inversion, pCR2.1-*Cry1* intron 336 R2 inversion, and pCR2.1-*Cry1* intron 336 R1,2 inversion (see above), and pMU2-P(*Cry1*)-*Cry1* plasmid (see above). The various *Cry1* intron 336 fragments were ligated at the *I-Sce*I site of pMU2-P(*Cry1*)-*Cry1*, and designated as pMU2-P(*Cry1*)-*Cry1* intron 336-*Cry1*, pMU2-P(*Cry1*)-*Cry1* intron 336 R1 deletion-*Cry1*, pMU2-P(*Cry1*)-*Cry1* intron 336 R2 deletion-*Cry1*, pMU2-P(*Cry1*)-*Cry1* intron 336 R1,2 deletion-*Cry1*, pMU2-P(*Cry1*)- *Cry1* intron 336 R1 mutation-*Cry1*, pMU2-P(*Cry1*)-*Cry1* intron 336 R2 mutation-*Cry1*, pMU2-P(*Cry1*)-*Cry1* intron 336 R1,2 mutation-*Cry1*, pMU2-P(*Cry1*)-*Cry1* intron 336 R1 inversion-*Cry1*, pMU2-P(*Cry1*)-*Cry1* intron 336 R2 inversion-*Cry1*, and pMU2- P(*Cry1*)-*Cry1* intron 336 R1,2 inversion-*Cry1*, respectively.

pMU2-P(Cry1)-Cry1 Intron 336-Cry1-Rluc and pMU2-P(Cry1)-Cry1 Intron 336 R1,2 Mutation-Cry1-Rluc

First, the coding sequence of *Renilla luciferase* (*Rluc*) was amplified from phRL-SV40 plasmid (Promega) using PCR with the following primers: Forward primers containing *PI-Psp*I recognition sequence: (5′-*TGGCAAACA GCTATTATGGGTATTATGGG T*GCTTCCAAGGTGTAC GACCCCGAGC-3′, recognition sequence is indicated with italics, Hokkaido System Science), Reverse primers containing *PI-Sce*I recognition sequence: (5′-*TGCCATTTCATTACCTCTTTCTCCGCACCCGACATAGAT*TTACTGCTC GTTCTTCAGCACGCGC-3′). PCR product was digested with *PI-Psp*I and *PI-Sce*I (New England BioLabs) and ligated at the *PI-Psp*I and *PI-Sce*I sites of pMU2-P(*Cry1*)-*Cry1* intron 336-*Luc* and pMU2-P(*Cry1*)-*Cry1* intron 336 R1,2 mutation-*Luc* (see above) to replace *Luc* fragment, and the resulting construct were designated as pMU2-P(*Cry1*)-*Cry1* intron 336-*Rluc* and pMU2-P(*Cry1*)-*Cry1* intron 336 R1,2 mutation-*Rluc*.

Next, the coding sequence of *Cry1* was amplified using PCR with the following primers: Forward primers containing *PI-Psp*I recognition sequence: (5′-*TGGCAAACAGCTATTATGGGTATTATGGGT*GGGGTGAACGCCGTGCAC-3′), Reverse primers containing *PI-Psp*I recognition sequence: (5′-*ACCCATAATACCCATAATAGCTGTTTGCCA*GTTACTGCTCTGCCGCTGG-3′). PCR product was digested with *PI-Psp*I and ligated at the *PI-Psp*I site of pMU2-P(*Cry1*)-*Cry1* intron 336-*Rluc* and pMU2-P(*Cry1*)-*Cry1* intron 336 R1,2 mutation-*Rluc*, and the resulting construct were designated as pMU2-P(*Cry1*)-*Cry1* intron 336-*Cry1*-*Rluc* and pMU2-P(*Cry1*)-*Cry1* intron 336 R1,2 mutation-*Cry1*-*Rluc*.

pLV7-P(Cry1)-Cry1 Intron 336-Cry1 and pLV7-P(Cry1)-Cry1

For generation of lentiviral constructs, the *Cry1* cDNA with or without 336bp of *Cry1* intron sequence was first cloned into pENTR-D entry vector (Invitrogen), and the *Cry1* promoter was cloned into pENTR-5′ vector (Invitrogen). The pENTR/D-cDNA and pENTR-5′-promoter plasmid DNAs were then recombined with pLenti6/R4R2/V5-DEST destination vector (Invitrogen) in a Gateway

recombination reaction to generate lentiviral expression constructs. Vector construction, lentivirus production, and infection into $Cry1^{-/-}$:

$Cry2^{-/-}$:$Per2^{Luc}$ cells were done as previously described (Liu et al., 2008; Liu et al., 2007). Infected cells were selected with blasticidin for 3-7 days prior to bioluminescence recording on a LumiCycle (Actimetrics).

pMU2-2 × RRE-P(Cry1)-Cry1

We used inverse PCR to fuse two tandem repeats of *Bmal1* RRE element to P(*Cry1*). For construction, we used pMU2-P(*Cry1*)-*Cry1* (see above) as a template with the following primers: Forward primers: (5′-AGGCAGAAAG TAGGTCAGGGACGCTGTTGGGAAGGG CGATCGGGTACC-3′, Hokkaido System Science), Reverse primers: (5′-CGTCCCTGACCTACTTTCTGCCTTTGCGCAGCCT GAATGGCGAATGGG-3′). Inverse PCR products were treated with Mighty Cloning kit (TaKaRa) for 5′-end phosphorylation, and subsequently self-ligated, and designated as pMU2-2 × RRE-P(*Cry1*)-*Cry1*.

pMU2-P(SV40)-Cry2

We amplified the full-length coding sequence of mouse *Cry2* from pCI-*Cry2* by PCR with forward primers containing *PI-Psp*I recognition sequence (5′-*TGGCAAACAGCTATTATGGGTATTATGGGT*GCGGCGGCTGCTGTGGTG-3′, recognition sequence is indicated with italics, Hokkaido System Science) and reverse primers containing *PI-Sce*I recognition sequence (5′-*TGCCATTTCATTACCT CTTTCTCCGCACCCGACATAGAT*TCAGGAGTCCTTGCTTGCTG-3′). PCR product was digested with *PI-Psp*I and *PI-Sce*I (New England BioLabs) and cloned into pMU2-P(SV40)-*Luc* vector (see above) instead of *Luc* gene, and the resulting construct was designated as pMU2-P(SV40)-*Cry2*.

pMU2-2 × D Box-P(SV40)-Luc, pMU2-1 × D Box-P(SV40)-Luc, pMU2-2 × Cry1proD- P(SV40)-Luc, and pMU2-1 × Cry1proD-P(SV40)-Luc

Oligonucleotides (Hokkaido System Science) containing one or two tandem repeats of *Per3* D box or Cry1proD elements were annealed, and inserted into the *Mlu*I-BglII site upstream of SV40 basic promoter of pMU2-P(SV40)-*Luc* (see above), and the resulting constructs were designated as pMU2-2 × D box-P(SV40)-*Luc*, pMU2-1 × D box-P(SV40)-*Luc*, pMU2- 2 × Cry1proD-P(SV40)-*Luc*, pMU2-1 × Cry1proD-P(SV40)-*Luc*.

Oligonucleotide Sequences for One or Two Tandem Repeats of D Box or Cry1proD Element
One D Box Element

Forward oligonucleotide, 5′-CGCGCCCGCGCGTTATGTAAGGTACTCG-3′; reverse, 5′-GATCCGAGTACCTTACATAACGCGC GGG-3′.

Two Repeats of D Box Element

Forward oligonucleotide, 5′-CGCGCCCGCGCGTTATGTAAGGTACTCGCCCGCGCGTTATGTAAGGTACTCG-3′; reverse, 5′-GAT CCGAGTACCTTACATAACGCGCGGGCGAGTACCTTACATAACGCGCGGG-3′.

One Time of Cry1proD Element

Forward oligonucleotide, 5′-CGCGAAACACACTTCAGAAACGTGAGGT-3′; reverse, 5′-GATCACCTCACGTTTCTGAAGTGTG TTT-3′.

Two Repeats of Cry1proD Element

Forward oligonucleotide, 5′-CGCGAAACACACTTCAGAAACGTGAGGTAAACACACTTCAGAAACGTGAGGT-3′; reverse, 5′-GATC ACCTCACGTTTCTGAAGTGTGTTTACCTCACGTTTCTGAAGTGTGTTT-3′.

pMU2-2 × D Box-P(SV40)-Cry1 Intron 336-Luc, pMU2-1 × D Box-P(SV40)-Cry1 Intron 336-Luc, pMU2-3 × Cry1proD-P (SV40)-Cry1 Intron 336-Luc, pMU2-2 × Cry1proD-P(SV40)-Cry1 Intron 336-Luc, and pMU2-1 × Cry1proD-P(SV40)- Cry1 Intron 336-Luc

pCR2.1-*Cry1* intron 336 (see above) was digested with *I-Sce*I. pMU2-2 × D box-P(SV40)-*Luc*, pMU2-1 × D box-P(SV40)-*Luc*, pMU2-3 × Cry1proD-*Luc*, pMU2-2 × Cry1proD-P(SV40)-*Luc*, pMU2-1 × Cry1proD-P(SV40)-*Luc* plasmids (see above) were also digested with *I-Sce*I. *Cry1* intron 336 fragment was ligated at the *I-Sce*I site of these plasmids, and designated as pMU2-2 × D box-P(SV40)-*Cry1* intron 336-*Luc*, pMU2-1 × D box-P(SV40)-*Cry1* intron 336-*Luc*, pMU2-3 × Cry1proD-P(SV40)- *Cry1* intron 336-*Luc*, pMU2-2 × Cry1proD-P(SV40)-*Cry1* intron 336-*Luc* and pMU2- 1 × Cry1proD-P(SV40)-*Cry1* intron 336-*Luc*, respectively.

pMU2-P(SV40)-Cry1 Intron 336-Cry1, pMU2-3 × D Box-P(SV40)-Cry1 Intron 336-Cry1, pMU2-2 × D Box-P(SV40)-Cry1 Intron 336-Cry1, pMU2-1 × D Box-P(SV40)-Cry1 Intron 336-Cry1, pMU2-3 × Cry1proD-P(SV40)-Cry1 Intron 336-Cry1, pMU2-2 × Cry1proD-P(SV40)-Cry1 Intron 336-Cry1, and pMU2-1 × Cry1proD-P(SV40)-Cry1 Intron 336-Cry1

pMU2-P(*Cry1*)-*Cry1* (see above) was digested with *PI-Psp*I and *PI-Sce*I, and the *Cry1* fragment was cloned into pMU2-P(SV40)-*Cry1* intron 336-*Luc*, pMU2-3 × D box-P(SV40)-*Cry1* intron 336-*Luc*, pMU2-2 × D box-P(SV40)- *Cry1* intron 336-*Luc*, pMU2-1 × D box-P (SV40)-*Cry1* intron 336-*Luc*, pMU2-3 × Cry1proD-P(SV40)-*Cry1* intron 336-*Luc*, pMU2-2 × Cry1proD-P(SV40)-*Cry1* intron 336-*Luc*, pMU2-1 × Cry1proD-P(SV40)-*Cry1* intron 336-*Luc* vector (see above) in replace of the *Luc* gene, and the resulting constructs were designated as pMU2- P(SV40)-*Cry1* intron 336-*Cry1*, pMU2-3 × D box-P(SV40)-*Cry1* intron 336-*Cry1*, pMU2-2 × D box-P(SV40)- *Cry1* intron 336-*Cry1*, pMU2-1 × D box-P(SV40)-*Cry1* intron 336-*Cry1*, pMU2-3 × Cry1proD-P(SV40)-*Cry1* intron 336-*Cry1*, pMU2-2 × Cry1proD- P(SV40)-*Cry1* intron 336-*Cry1* and pMU2-1 × Cry1proD-P(SV40)-*Cry1* intron 336-*Cry1*, respectively.

pMU2-P(TKms)-Cry1 and pMU2-P(TKms)-Cry1 Intron 336-Cry1

TKms promoter fragment (short sequence of TK promoter) (gift from Dr. H. Ukai, 5′-GTCCCAGGT CCACTTCGCATATTAAGGTG ACGCGTGTGGCCTCGAA-3′) was cloned into the KpnI-*Hind*III sites of pMU2-P(SV40)-*Cry1* and pMU2-P(SV40)-*Cry1* intron

336-*Cry1* vectors (see above) in replace of P(SV40) promoter, and designated as pMU2- P(TKms)-*Cry1* and pMU2-P(TKms)-*Cry1* intron336-*Cry1*.

pMU2-P(SV40)-Cry1 Intron 336-Cry1-Rluc

First, the coding sequence of *Renilla luciferase* (*Rluc*) was amplified from phRL-SV40 plasmid (Promega) using PCR with the following primers: Forward primers containing *PI-Psp*I recognition sequence: (5′-*T GGCAAACAGCTATTATGGGTATTATGG GT*GCTTCCAAGGTGTACGACCCCGAGC-3′, recognition sequence is indicated with italics, Hokkaido System Science), Reverse primers containing *PI-Sce*I recognition sequence: (5′-*TGCCATTTCATTACC TCTTTCTCCGCACCCGACATAGAT*TTACTGCTC GTTCTTCAGCACGCGC-3′). PCR product was digested with *PI-Psp*I and *PI-Sce*I (New England BioLabs) and ligated at the *PI-Psp*I and *PI-Sce*I sites of pMU2-P(SV40)-*Cry1* intron 336-*Luc* (see above) to replace *Luc* fragment, and the resulting construct were designated as pMU2-P(SV40)-*Cry1* intron 336-*Rluc*.

Next, the coding sequence of *Cry1* was amplified using PCR with the following primers: Forward primers containing *PI-Psp*I recognition sequence: (5′-*TGG CAAACAGCTATTATGGGTATTATGGGT*GGGGTGAACGCCGTGCAC-3′), Reverse primers containing *PI-Psp*I recognition sequence: (5′-*ACCCATAATACCCATAATAG CTGTTT GCCA*GTTACTGCTCTGCCGCTGG-3′). PCR product was digested with *PI-Psp*I and ligated at the *PI-Psp*I site of pMU2-P(SV40)-*Cry1* intron 336-*Rluc*, and the resulting construct were designated as pMU2-P(SV40)-*Cry1* intron 336-*Cry1*-*Rluc*.

pMU2-P(SV40)-Cry1 Intron 336 R1,2 Mutation-Cry1

pCR2.1-*Cry1* intron 336 R1,2 mutation (see above) was digested with *I-Sce*I. The *Cry1* intron 336 R1,2 mutation fragment was ligated at the *I-Sce*I site of pMU2-P(SV40)-*Cry1* intron 336-*Cry1* plasmid (see above) to replace the *Cry1* intron 336 fragment, and the resulting construct was designated as pMU2-P(SV40)-*Cry1* intron 336 R1,2 mutation-*Cry1*.

Bioinformatics Search for Potential Clock-Controlled Elements

We comprehensively examined conserved regions in the *Cry1* promoter sequence and the 1st intron sequence for potential clock controlled elements using a Bioinformatics approach. Genomic sequence data and evolutionary conserved region data were obtained from UCSC Genome Browser (Rhead et al., 2010; Siepel et al., 2005). There are 5 conserved regions in *Cry1*'s promoter and 23 regions in the 1st intron sequence. The first and second most closely resembling D box sequences were found in *Cry1* promoter by using position weight matrix analysis with MA0025 of JASPAR database (Bryne et al., 2008). Two consensus RRE sequences were found in the 1st intron by regular expression analysis of Perl script language.

Rhythmicity, Period Length, Phase, and Relative Amplitude Analysis of Real-Time Bioluminescence Data

The rhythmicity and period length of the promoter activity for each reporter were determined as described previously (Sato et al., 2006), with a slight change. Briefly, Bioluminescence time-series data beginning 21 hr after forskolin stimulation were used for analysis in order to distinguish endogenous circadian oscillation from acute effects of stimulation. Bioluminescence data were detrended using the trend curve calculated by smoothing spline method. The smoothing parameter for this calculation was set such that its frequency-response was 33% at the frequency of about 2 cycles (42 hr) of the typical circadian period (~21 hr) observed in fibroblasts transfected with an empty vector at 30°C. Then, autocorrelation of the detrended bioluminescence time-series data was calculated within the range of 15-36 hr to determine the circadian period of oscillation. Statistical significance (p = 0, most significant to 1, least significant) of circadian oscillation was evaluated by comparing the strongest autocorrelation of the detrended data within the range of 15-36 hr against that of white-noise (theoretical value for the autocorrelation of white noise is $-1/N \pm 1/\sqrt{N}$, mean ± SD, where N is the number of time points). To calculate the phase, a cosine wave with the period corresponding to the maximum autocorrelation in the range, was fitted to the detrended bioluminescence data. The calculated phase was scaled to the phase in 24 hr period, for phase comparison of different period waves.

To calculate the relative amplitude of bioluminescence data, the moving average of the absolute value of the detrended bioluminescence was calculated first. The window size of the moving average was set to half of the estimated period. Then, the moving averaged data was smoothened by the smoothing spline method resulting in the amplitude trend. The amplitude trend was then divided by the trend curve of the original time-series at each time point to be used as the relative amplitude.

Periodogram and Significance Test

For drawing periodogram, time-series data of bioluminescence was detrended by subtracting trend curve. The detrended time-series was divided by standard deviation for normalization. The trend curve was estimated by smoothing spline method as described in the previous sub-section. Then, inner-products of the detrended time-series with cosine and sine waves were evaluated. Before taking inner-product, the cosine and sine waves were scaled so that their norm was 1. Amplitude of time-series at each period component was evaluated as square-root of sum-of-squared those two inner-products. The amplitudes are plotted against periods of the sine and cosine waves varying with 0.1 hr interval from 5 to 34 hr. For statistical test of ~11 hr periodicity, amplitudes of the harmonic periods in the range of 8~14 hr were extracted. The sum-of-squared amplitude of those harmonic periods was compared against *chi*-square distribution for statistical test.

Phase Vector and Addition of Waves

The addition of multiple trigonometric waves with same frequency results in a trigonometric wave of same frequency with a novel phase. This can be shown as follows.

Assume we have two wave functions $f_1(t), f_2(t)$:

$$f_1(t) = A_1 \cos(\theta(t) + \phi_1)$$
$$f_2(t) = A_2 \cos(\theta(t) + \phi_2)$$

where A_1 and A_2 are amplitudes, ϕ_1 and ϕ_2 are phases of corresponding waves, $\theta(t)$ is angle which depends on time: t.

Then the summed function $f_c(t)$ of these two waves is derived by using formulae of "angle sum and difference identities" and "linear combination":

$$f_c(t) = A_c \cos(\theta(t) + \phi_c)$$

where

$$A_c = \sqrt{(A_1 \cos(\phi_1) + A_2 \cos(\phi_2))^2 + (A_1 \sin(\phi_1) + A_2 \sin(\phi_2))^2},$$

$$\cos(\phi_c) = \frac{(A_1 \cos(\phi_1) + A_2 \cos(\phi_2))}{\sqrt{(A_1 \cos(\phi_1) + A_2 \cos(\phi_2))^2 + (A_1 \sin(\phi_1) + A_2 \sin(\phi_2))^2}},$$

$$\sin(\phi_c) = \frac{(A_1 \sin(\phi_1) + A_2 \sin(\phi_2))}{\sqrt{(A_1 \cos(\phi_1) + A_2 \cos(\phi_2))^2 + (A_1 \sin(\phi_1) + A_2 \sin(\phi_2))^2}}$$

On the other hand, the two waves can be represented as phase vectors where the phase and amplitude of a wave are represented by the direction and length of a vector, respectively. In Figure S7B, *wave1* and *wave2* are respectively represented as red and blue phase vectors. Coordinates of the two phase vectors: P_1 and P_2 are $(A_1 \cos(\phi_1), A_1 \sin(\phi_1))$ and $(A_2 \cos(\phi_2), A_2 \sin(\phi_2))$; summed phase vector: P_c 's coordinate is $(A_1 \cos(\phi_1) + A_2 \cos(\phi_2), A_1 \sin(\phi_1) + A_2 \sin(\phi_2))$. In this phase vector, P_c represents the wave with amplitude $A_c' = \sqrt{(A_1 \cos(\phi_1) + A_2 \cos(\phi_2))^2 + (A_1 \sin(\phi_1) + A_2 \sin(\phi_2))^2}$ and phase ϕ_c' such that

$$\cos(\phi_c') = \frac{(A_1 \cos(\phi_1) + A_2 \cos(\phi_2))}{\sqrt{(A_1 \cos(\phi_1) + A_2 \cos(\phi_2))^2 + (A_1 \sin(\phi_1) + A_2 \sin(\phi_2))^2}}$$

$$\sin(\phi_c') = \frac{(A_1 \sin(\phi_1) + A_2 \sin(\phi_2))}{\sqrt{(A_1 \cos(\phi_1) + A_2 \cos(\phi_2))^2 + (A_1 \sin(\phi_1) + A_2 \sin(\phi_2))^2}}.$$

This means $A_c = A_c'$ and $\phi_c = \phi_c'$, i.e., the summed phase vector represents the wave of $f_c(t)$.

Period of Negative Feedback Loop with Time Delay

There is an excellent review which succinctly described basic properties of negative feedback loop with time delay (Novak and Tyson, 2008). Here, we adopt their mathematical model, and present the relation between the oscillation period and the time delay by supplementing their derivation.

The model of the delayed negative feedback loop in the review can be interpreted in terms of delayed repression onto its own transcriptional regulatory element (Figure S7C). The mathematical description of the model:

$$\frac{dY(t)}{dt} = k_1 S \frac{K_d^p}{K_d^p + Y(t-\tau)^p} - k_2 E_T \frac{Y(t)}{K_m + Y(t)} \tag{1}$$

can be regarded as, Y(t) is the concentration of the repressor protein at time t, S is the activator concentration, K_d is the dissociation constant for the repressor protein with the regulatory element, E_T is the concentration of a protease that degrades the repressor protein, K_m is Michaelis constant of the degradation reaction, k_1 and k_2 are the synthesis and the degradation rate of the repressor protein respectively, p is Hill coefficient, and τ is the time delay.

In numerical simulations of the model (1) with parameters: $k_1 = 1$, $k_2 = 1$, $S = 2$, $K_d = 1$, $E_T = 1$, $K_m = 0.1$, $p = 2$, $\tau = 1, 3,$ or 6, we see that the period of oscillation becomes longer as the time delay becomes larger (Figure S7D). Note that under a critical value

of time delay τ which is $1 < \tau < 3$ in this case, the model is stable and does not display sustained oscillation. Here, we first intend to find the constraint on the time delay for a sustained oscillation, and then we seek to approximately describe the relation between the oscillation period and the time delay.

The model Equation (1) can be formatted as

$$\frac{K_d}{k_2 E_T} \frac{d\left\{\frac{Y(t)}{K_d}\right\}}{dt} = \frac{k_1 S}{k_2 E_T} \frac{1}{1 + \left\{\frac{Y(t-\tau)}{K_d}\right\}^p} - \frac{\left\{\frac{Y(t)}{K_d}\right\}}{\frac{K_m}{K_d} + \left\{\frac{Y(t)}{K_d}\right\}}$$

By introducing variables $\sigma = k_1 S / k_2 E_T, \kappa = K_m / K_d, y(\hat{t}) = Y(t)/K_d$ and $\hat{t} = (k_2 E_T / K_d)t$, we obtain a dimensionless form of (1)

$$\frac{dy(\hat{t})}{d\hat{t}} = \frac{\sigma}{1 + \{y(\hat{t} - \hat{\tau})\}^p} - \frac{y(\hat{t})}{\kappa + y(\hat{t})}. \tag{3}$$

The properties of this equation can be analyzed around the fixed points (steady points). The fixed points can be obtained as in the case of non-delayed differential equation, because $y(\hat{t}) = y(\hat{t} - \hat{\tau})$ at fixed points. A fixed point y_0 is a positive real root of the equation

$$y^{p+1} - (\sigma - 1)y - \sigma\kappa = 0 \tag{4}$$

which is given by setting $dy(\hat{t})/d\hat{t} = 0$ in (3).

To investigate a solution around the fixed point, the Equation (3) is linearized around y_0 by Taylor expansion

$$\frac{dy(\hat{t})}{d\hat{t}} = -\frac{\sigma p y_0^{p-1}}{\left(1 + y_0^p\right)^2}\{y(\hat{t} - \hat{\tau}) - y_0\} - \frac{\kappa}{(\kappa + y_0)^2}\{y(\hat{t}) - y_0\} \tag{5}$$

Assuming $y(\hat{t}) = y_0 + e^{\lambda\hat{t}}$ in (5), the characteristic equation is obtained

$$\lambda + \frac{\sigma p y_0^{p-1}}{\left(1 + y_0^p\right)^2}e^{-\lambda\hat{\tau}} + \frac{\kappa}{(\kappa + y_0)^2} = 0 \tag{6}$$

This Equation (6) states that the real part of λ is negative when there is no time delay: $\hat{\tau} = 0$, because

$$\lambda = -\frac{\sigma p y_0^{p-1}}{\left(1 + y_0^p\right)^2} - \frac{\kappa}{(\kappa + y_0)^2} < 0 \tag{7}$$

Therefore, the solution of the model around y_0 is stable for $\hat{\tau} = 0$.

Let's assume there is a critical value of $\hat{\tau}$ at which the sign of the real part of λ changes from negative to positive as $\hat{\tau}$ increases. At the critical $\hat{\tau}$, the real part of λ is 0, and the model loses its stability (Hopf bifurcation). To find the critical $\hat{\tau}$, we substitute $\lambda = i\omega$ into (7), and obtain

$$i\omega + \frac{\sigma p y_0^{p-1}}{\left(1 + y_0^p\right)^2}(\cos(\omega\hat{\tau}) - i\sin(\omega\hat{\tau})) + \frac{\kappa}{(\kappa + y_0)^2} = 0. \tag{8}$$

In order for (8) to hold, the real and imaginary parts of (8) must be 0. By introducing variables $\rho = \kappa/(\kappa + y_0)^2$, $\phi = \sigma p y_0^{p-1}/(1 + y_0^p)^2$, and dealing the real and the imaginary part separately, we obtain

$$\text{Real} : \phi\cos(\omega\hat{\tau}) = -\rho \tag{9}$$

$$\text{Imaginary} : \phi\sin(\omega\hat{\tau}) = \omega \tag{10}$$

Squaring each (9) and (10) and summing them result in

$$\rho^2 + \omega^2 = \phi^2 \tag{11}$$

And dividing (10) by (9) yields

$$\hat{\tau} = \frac{\arctan\left(-\frac{\omega}{\rho}\right)}{\omega} \tag{12}$$

By deleting ω from (11) and (12) we arrive at the equation

$$\widehat{\tau} = \frac{\arctan\left(-\sqrt{\left(\frac{\phi}{\rho}\right)^2 - 1}\right)}{\rho\sqrt{\left(\frac{\phi}{\rho}\right)^2 - 1}} \tag{13}$$

This equation gives the critical value of $\widehat{\tau}$. With a larger time delay than the critical $\widehat{\tau}$, the model displays a sustained oscillation (**Figure S7E**, **F** top panels) (Novak and Tyson, 2008).

The period of oscillation with time delay near the critical $\widehat{\tau}$ can be roughly estimated by (9):

$$\omega = \frac{\arccos(-\rho/\phi)}{\widehat{\tau}} \text{ and } period = 2\pi/\omega \tag{14}$$

These are summarized as

$$period = \frac{2\pi}{\arccos(-\rho/\phi)}\widehat{\tau} \tag{15}$$

By using this equation with (13), we can visualize combinations of variables which can generate oscillation along with the associated period (Figures S7E and S7F top panels). Note that there is a proportional relation between the oscillation period and the time delay in this model, and the coefficient is in range of $2\sim4$:

$$period = (\text{constant of } 2\sim4)\,\widehat{\tau} \tag{16}$$

This is because that ϕ and ρ are both positive and $\phi > \rho$ (i.e., $\phi/\rho > 1$) according to (11), therefore $-1 < -\rho/\phi < 0$. This means that $\pi/2 < \arccos(-\rho/\phi) < \pi$ in (14). We should emphasize again that the period estimation by (15) deviates from actual values or estimation by numerical simulation, and the deviation becomes larger as $\widehat{\tau}$ becomes larger. This is because the Equation (15) strictly holds only on the critical $\widehat{\tau}$ (**Figure S7E**, **F** bottom panels).

We used xpp-aut (http://www.math.pitt.edu/$\sim$bard /xpp/xpp.html) for numerical simulation of the model (1).

Statistics and Significance Test for Correlation

For evaluation of correlation, linear fit of a first-order-polynomial was performed by the least square method. Statistical significance was evaluated by Pearson's correlation. Analysis was performed using Microsoft Excel or R version 2.8.1.

SUPPLEMENTAL REFERENCES

Bryne, J.C., Valen, E., Tang, M.H., Marstrand, T., Winther, O., da Piedade, I., Krogh, A., Lenhard, B., and Sandelin, A. (2008). JASPAR, the open access database of transcription factor-binding profiles: new content and tools in the 2008 update. Nucleic Acids Res. 36, D102–D106.

Kumaki, Y., Ukai-Tadenuma, M., Uno, K.-D., Nishio, J., Masumoto, K.-h., Nagano, M., Komori, T., Shigeyoshi, Y., Hogenesch, J.B., and Ueda, H.R. (2008). Analysis and synthesis of high-amplitude Cis-elements in the mammalian circadian clock. Proc. Natl. Acad. Sci. USA 105, 14946–14951.
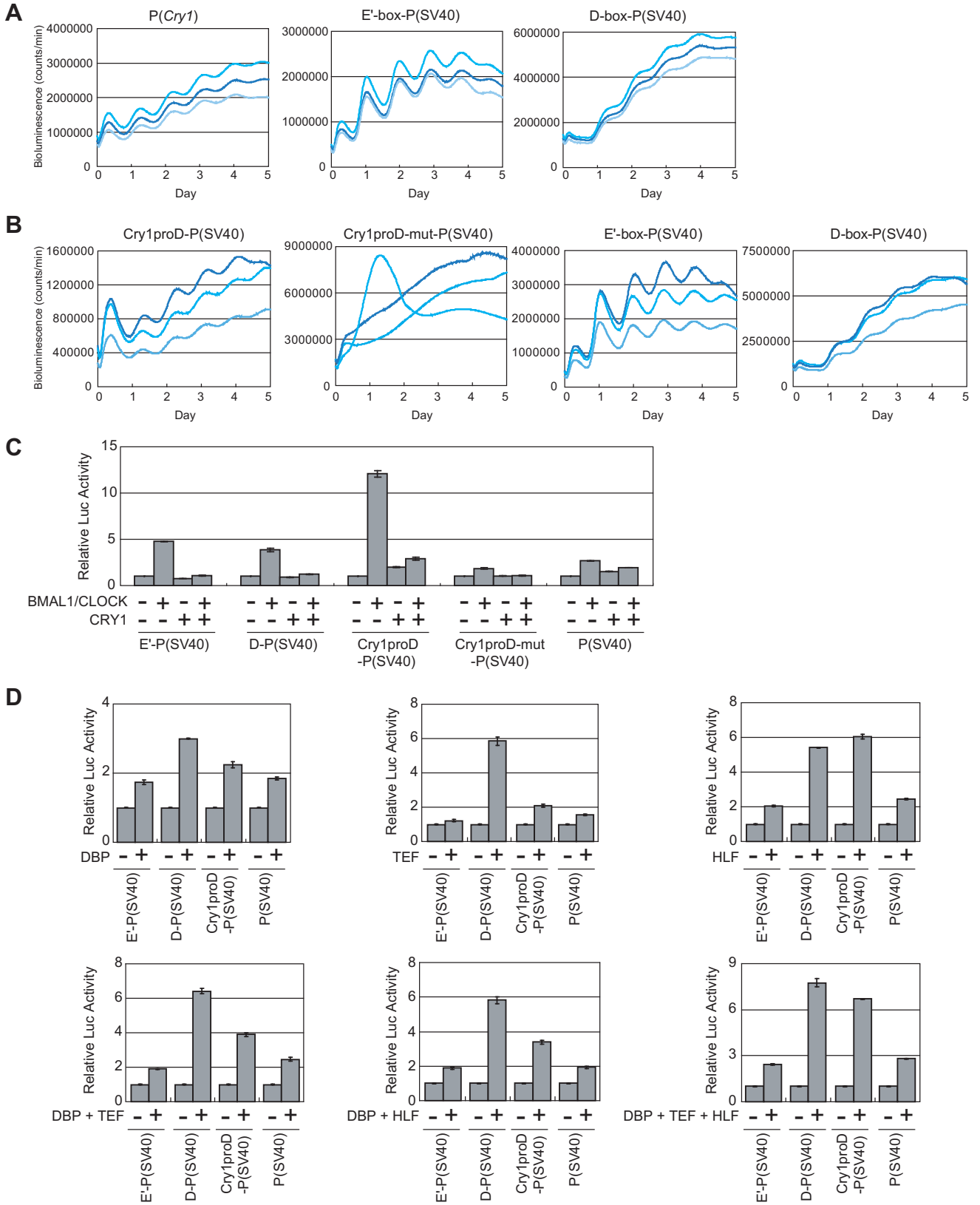
McCarthy, E.V., Baggs, J.E., Geskes, J.M., Hogenesch, J.B., and Green, C.B. (2009). Generation of a novel allelic series of cryptochrome mutants via mutagenesis reveals residues involved in protein-protein interaction and CRY2-specific repression. Mol. Cell. Biol. 29, 5465–5476.

Rhead, B., Karolchik, D., Kuhn, R.M., Hinrichs, A.S., Zweig, A.S., Fujita, P.A., Diekhans, M., Smith, K.E., Rosenbloom, K.R., Raney, B.J., et al. (2010). The UCSC Genome Browser database: update 2010. Nucleic Acids Res. 38, D613–D619.

Schmutz, I., Ripperger, J.A., Baeriswyl-Aebischer, S., and Albrecht, U. (2010). The mammalian clock component PERIOD2 coordinates circadian output by interaction with nuclear receptors. Genes Dev. 24, 345–357.

Siepel, A., Bejerano, G., Pedersen, J.S., Hinrichs, A.S., Hou, M., Rosenbloom, K., Clawson, H., Spieth, J., Hillier, L.W., Richards, S., et al. (2005). Evolutionarily conserved elements in vertebrate, insect, worm, and yeast genomes. Genome Res. 15, 1034–1050.

Wuarin, J., and Schibler, U. (1990). Expression of the liver-enriched transcriptional activator protein DBP follows a stringent circadian rhythm. Cell 63, 1257–1266.

A

P(*Cry1*) — Bioluminescence (counts/min) vs Day

E'-box-P(SV40) — Bioluminescence vs Day

D-box-P(SV40) — Bioluminescence vs Day

B

Cry1proD-P(SV40) — Bioluminescence (counts/min) vs Day

Cry1proD-mut-P(SV40) — Bioluminescence vs Day

E'-box-P(SV40) — Bioluminescence vs Day

D-box-P(SV40) — Bioluminescence vs Day

C

Relative Luc Activity

	E'-P(SV40)	D-P(SV40)	Cry1proD-P(SV40)	Cry1proD-mut-P(SV40)	P(SV40)
BMAL1/CLOCK	− + − +	− + − +	− + − +	− + − +	− + − +
CRY1	− − + +	− − + +	− − + +	− − + +	− − + +

D

Relative Luc Activity

DBP   − + − + − + − +   E'-P(SV40) D-P(SV40) Cry1proD-P(SV40) P(SV40)

TEF   − + − + − + − +   E'-P(SV40) D-P(SV40) Cry1proD-P(SV40) P(SV40)

HLF   − + − + − + − +   E'-P(SV40) D-P(SV40) Cry1proD-P(SV40) P(SV40)

DBP + TEF   − + − + − + − +   E'-P(SV40) D-P(SV40) Cry1proD-P(SV40) P(SV40)

DBP + HLF   − + − + − + − +   E'-P(SV40) D-P(SV40) Cry1proD-P(SV40) P(SV40)

DBP + TEF + HLF   − + − + − + − +   E'-P(SV40) D-P(SV40) Cry1proD-P(SV40) P(SV40)

Figure S1. Related to Figure 1

(A) Transcriptional activities of P(*Cry1*) (left), E' box-P(SV40) (middle) and D box-P(SV40) (right). Raw data of bioluminescence time-series corresponding to Figure 1A are shown (n = 3).

(B) Transcriptional activities of Cry1proD-P(SV40) (left), E' box-P(SV40) (middle) and D box-P(SV40) (right). Raw data of bioluminescence time-series corresponding to Figure 1D are shown (n = 3).

(C) The responsiveness of E' box, D box, Cry1proD, mutated Cry1proD, and SV40 promoters to clock factors. Reporters were constructed as in Figure 1F. Regulatory elements were activated by co-transfected E/E' box activator BMAL1/CLOCK and repressed by E/E' box repressor CRY1. Relative *Luciferase* activity for each promoter was scaled so that the activity with no transcriptional regulation is normalized to 1.

(D) The responsiveness of E' box, D box, Cry1proD, and SV40 promoters to clock factors. Regulatory elements were activated by co-transfected D box activators DBP, TEF or HLF, and their combinations DBP + TEF, DBP + HLF, or DBP + TEF + HLF. Relative *Luciferase* activity for each promoter was scaled so that the activity with no transcriptional regulation is normalized to 1. Error bars represent SD (n = 3). Data are representative of two independent experiments (A–D).

A

B

C
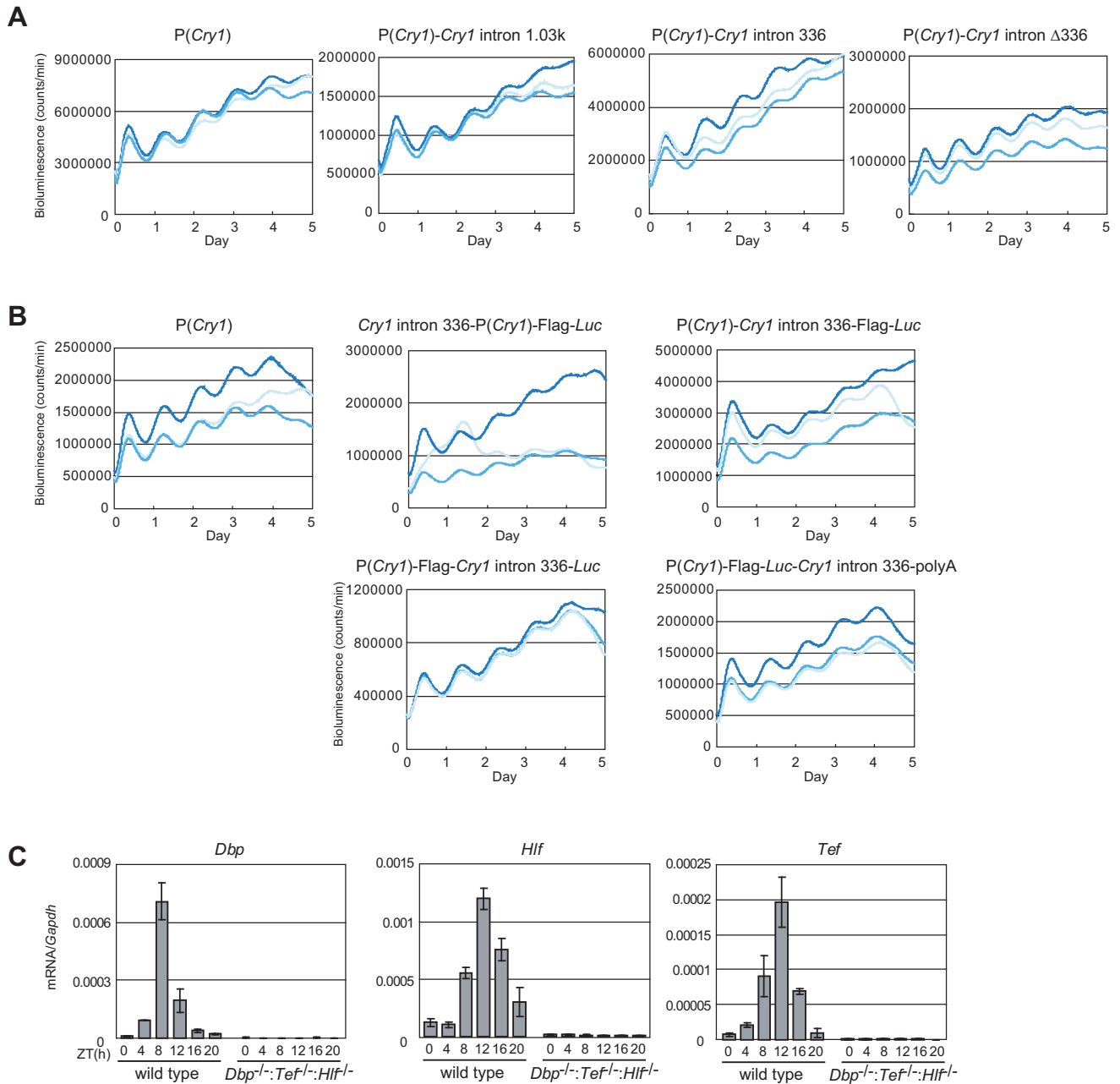
Figure S2. Related to Figure 2

(A) The *Cry1* promoter was combined with the 1.03 kbp of *Cry1* intron sequence, 336 bp of *Cry1* intron sequence, or *Cry1* intron Δ336 deletion mutant sequence to generate composite promoters, which were fused with a *Luciferase* reporter gene to generate reporter constructs. The reporter was then transiently transfected into NIH 3T3 cells followed by real-time bioluminescence recording. Raw data of bioluminescence time-series corresponding to Figure 2B are shown (n = 3).

(B) Transcriptional activity of *Cry1* promoter with 336 bp of *Cry1* intron sequence inserted into upstream or downstream of the *Cry1* promoter, and within or downstream of the *Luciferase* reporter coding sequence. Raw data of bioluminescence time-series corresponding to Figure 2C are shown (n = 3). Data are representative of two independent experiments (A and B).

(C) Circadian expression profiles of *Dbp*, *Tef* and *Hlf in vivo*. RNA from liver of wild-type (gray) or *Dbp*$^{-/-}$:*Tef*$^{-/-}$:*Hlf*$^{-/-}$ (orange) mice was prepared at 4 hr intervals from mice held in a 12 hr light-12 hr dark cycle (LD 12:12). Relative mRNA levels of each gene were measured by qPCR assay. All RNA samples were normalized to *Gapdh* mRNA accumulation. ZT: Zeitgeber time. Mean and SEM from two pools of three mice each per time point. The representative data from three independent experiments was shown.

A

B
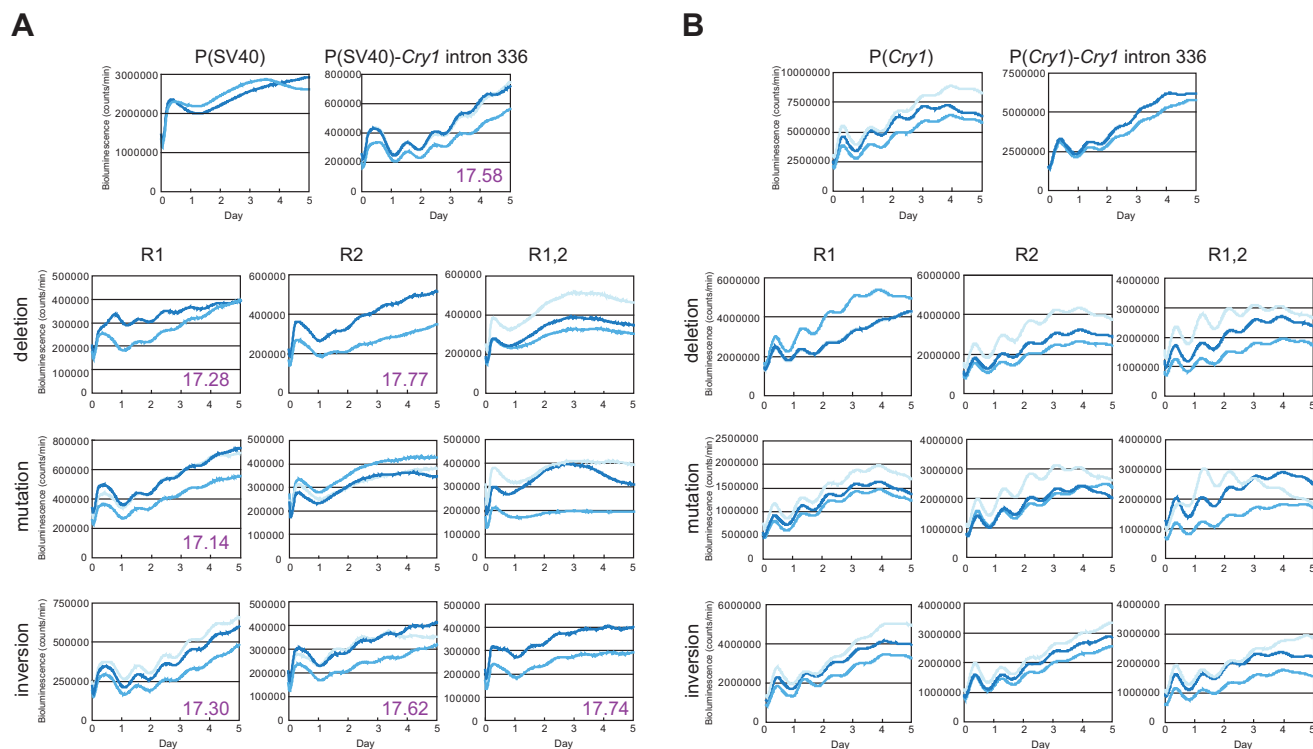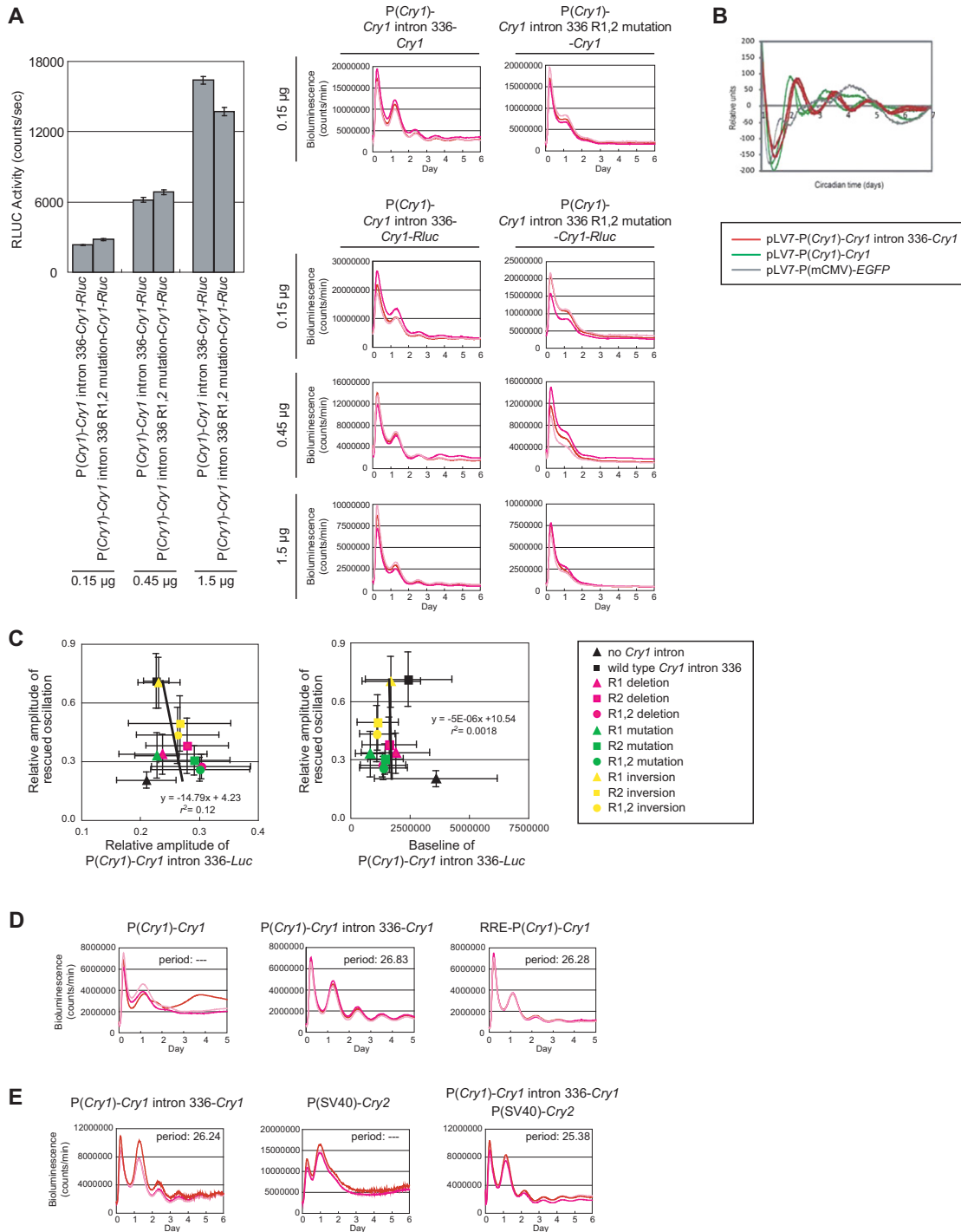

Figure S3. Related to Figure 3

(A) Transcriptional activities of various P(SV40)-*Cry1* intron 336-*Luc* constructs. Raw data of bioluminescence time-series corresponding to Figure 3C are shown. In the independent measurement for the strength of intronic RREs, we examined the amplitude of circadian oscillations expressed by the constructs in reporter rhythm assays. Bioluminescence levels from the control reporter construct, P(SV40)-Cry1 intron 336-Luc harboring an SV40 basic promoter and the intact 336 bp of the Cry1 intron sequence, were rhythmic and peaked at CT17.58 ± 0.52. As expected, circadian oscillation was not readily detectable for constructs with R1,2 deletion or R1,2 mutation. Most other mutant constructs (except R2 mutation) displayed significant circadian oscillations in bioluminescence, with phases not too different from the control, all peaking around CT17-18. Average phase of circadian oscillation is shown in each panel if the rhythmicity is significant.

(B) Transcriptional activities of various P(Cry1)-Cry1 intron 336-Luc constructs. To examine how intronic RRE mutation affects phase delay, we replaced the SV40 basic promoter in the P(SV40)-Cry1 intron 336-Luc vector with the Cry1 promoter, P(Cry1), to obtain an array of reporter constructs, namely P(Cry1)-Cry1 intron 336-Luc, each carrying different intronic RRE mutations as described in Figure 3E. Individual constructs were transfected into NIH 3T3 cells and bioluminescence levels in the transfected cells were monitored in real time, from which the phases of circadian oscillation were obtained (see also Figure 3E and Table S1). Raw data of bioluminescence time-series corresponding to Figure 3E are shown. Data are representative of two independent experiments (A and B).
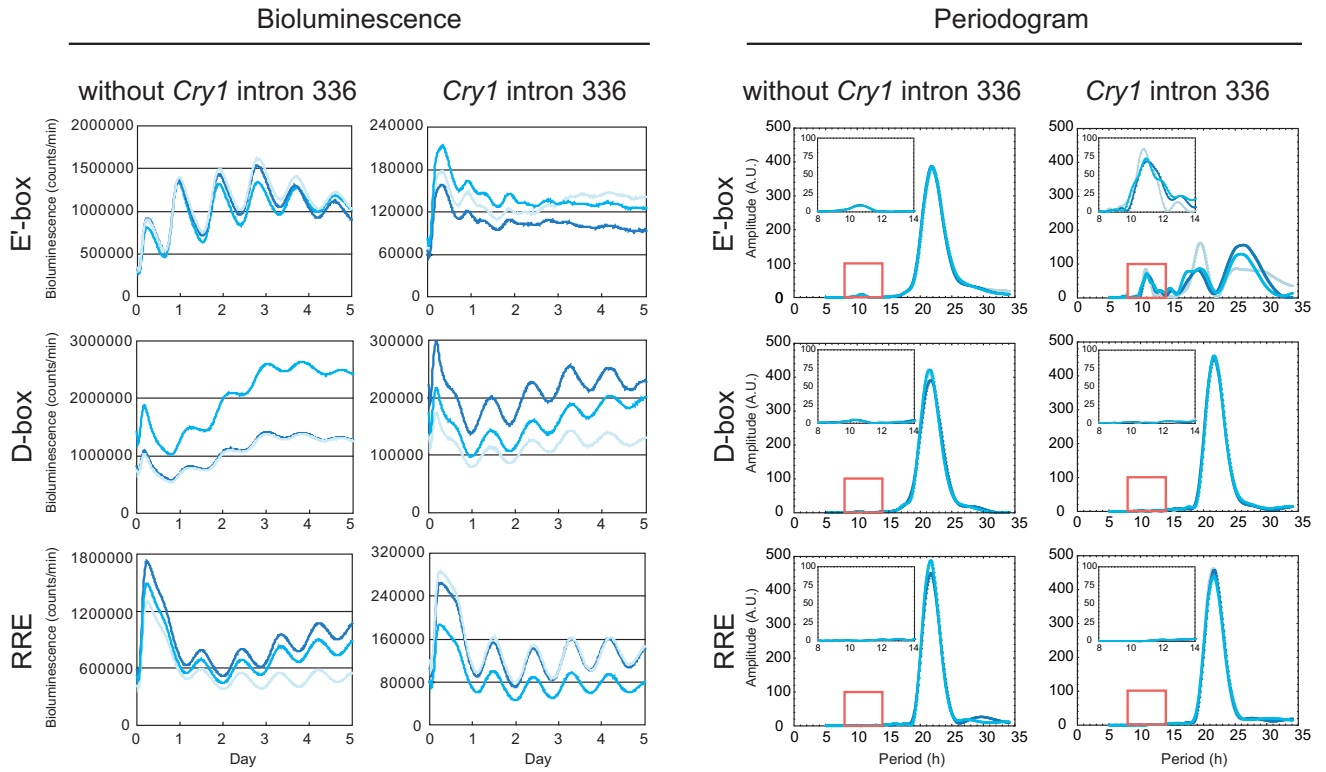
Figure S4. Related to Figure 4

(Left) Transcriptional activities of E' box, D box or RRE promoter with or without the 336 bp of *Cry1* intron sequence ("*Cry1* intron 336"). Raw data of bioluminescence time-series corresponding to Figure 4A are shown (n = 3). Data are representative of two independent experiments. (Right) Periodograms of time-series data presented on the left. Amplitude of corresponding period component of time-series data is plotted. Periods ranging 8∼14 hr are zoomed in and displayed in insets. Notably, only a composite promoter with E' box and *Cry1* intron 336 induced significant amplitude within this range (p < 0.01). Data are representative of two independent experiments.

Figure S5. Related to Figure 5

(A) Circadian oscillations in $Cry1^{-/-}:Cry2^{-/-}$ cells rescued by $Cry1$-Renilla luciferase ($Rluc$) fusion gene. To confirm that the observed rescue capability was independent of the CRY1 protein level, we employed a CRY1-Rluc (Renilla Luciferase) fusion protein in which the protein expression level in $Cry1^{-/-}:Cry2^{-/-}$ cells can be quantitatively measured through a bioluminescence assay (McCarthy et al., 2009). We generated $Cry1$ rescue constructs, in which $Cry1$-$Rluc$ is driven by the combination of the $Cry1$ promoter with either wild-type or mutated $Cry1$ intron sequence. $Cry1^{-/-}:Cry2^{-/-}$ cells were transiently co-transfected with P($Per2$)-dLuc, and various amounts (up to 10-fold) of $Cry1$-$Rluc$ driven by P($Cry1$) with wild-type or R1,2 mutation of 336bp of $Cry1$ intron sequence. The RLUC activities of each sample were measured (left). P($Per2$)-dLuc reporter activity in transfected $Cry1^{-/-}:Cry2^{-/-}$ cells expressing either $Cry1$ (top) or $Cry1$-$Rluc$ (bottom) was recorded (n = 3). $Cry1$ expression was under the control of either a wild-type (middle) or R1,2 mutation (right) of 336bp of $Cry1$ intron sequence. The results indicate that the differences in protein expression level among the constructs are relatively smaller compared to those in DNA amounts used in transfection.

Nevertheless, all three tested DNA amounts rescued circadian rhythms and only the constructs containing wild-type intron sequence were able to reliably rescue rhythmicity with comparable amplitude. Error bars represent SD (n = 3).

(B) Representative records of bioluminescence rhythms in $Cry1^{-/-}$:$Cry2^{-/-}$:$Per2^{Luc}$ cells through cellular genetic complementation. Lentiviral expression vectors carrying $Cry1$ under the control of P($Cry1$) in the presence or absence of the 336 bp of $Cry1$ intron sequence were introduced into $Cry1^{-/-}$:$Cry2^{-/-}$:$Per2^{Luc}$ cells. GFP was used as a negative control. Bioluminescence expression was recorded on a LumiCycle device (Actimetrics Inc.) and representative plots using baseline-subtracted bioluminescence data are shown. The results indicate that the rescue capability was also independent of vector type or method of DNA delivery. Mean and SD (error bar) of two independent experiments are shown (each experiment contains three samples; n = 3 unless otherwise indicated in Table S1).

(C) Rescue capability does not correlate with either amplitude (left) or basal (right) bioluminescence levels of P($Cry1$)-$Cry1$ intron 336-Luc. The relative amplitudes of circadian oscillations in $Cry1^{-/-}$:$Cry2^{-/-}$ cells rescued by P($Cry1$)-$Cry1$ intron 336-$Cry1$ are plotted against the relative amplitude (left) and the baseline (right) of various P($Cry1$)-$Cry1$ intron 336-Luc activity presented in Figure S3B. Mean and SD (error bar) of two independent experiments are shown (each experiment contains three samples; n = 3).

(D) Circadian oscillations in $Cry1^{-/-}$:$Cry2^{-/-}$ cells rescued with $Cry1$ driven by 2 tandem copies of RRE which were fused to P($Cry1$). $Cry1^{-/-}$:$Cry2^{-/-}$ cells were transiently co-transfected with P($Per2$)-dLuc and $Cry1$ gene driven by P($Cry1$) (left), P($Cry1$) and $Cry1$ intron 336 sequence (middle), or RRE (from $Bmal1$) fused to P($Cry1$) (right).

(E) Circadian rhythmicity in $Cry1^{-/-}$:$Cry2^{-/-}$ cells rescued with $Cry1$ and $Cry2$. The $Cry1$-rescued $Cry1^{-/-}$:$Cry2^{-/-}$ cells (a $Cry2$ knockout, in essence) showed a rather long period length of ~27 hr (see also Figure 5A and Table S3), which is consistent with previous reports showing that $Cry2^{-/-}$ single knockout cells display long periods compared to wild-type cells (~24-25 hr) (Liu et al., 2007). Since $Cry2$ expression does not show robust circadian oscillation in SCN or any of the examined peripheral tissues (Kume et al., 1999), we hypothesized that we could achieve double rescue by introducing $Cry2$ under a constitutive promoter in $Cry1$-rescued $Cry1^{-/-}$:$Cry2^{-/-}$ cells. To test this, $Cry1^{-/-}$:$Cry2^{-/-}$ cells were transiently co-transfected with P($Per2$)-dLuc, and P($Cry1$)-$Cry1$ intron 336-$Cry1$ (left), P(SV40)-$Cry2$ (middle), or both (right). The period of $Cry1^{-/-}$:$Cry2^{-/-}$ cells rescued with both $Cry1$ and $Cry2$ was 25.38 ± 0.06 hr (see also Table S3), which was significantly shorter than $Cry1$ rescue alone (p < 0.05, Welch's t test) and close to the natural period of WT cells. These results support the notion that genetic complementation of $Cry1$ in $Cry1^{-/-}$:$Cry2^{-/-}$ cells recapitulates the circadian phenotype in $Cry2$ single knockout cells, thus phenotypically validating the $Cry1$ rescue assay. Data are representative of two independent experiments (A–E).
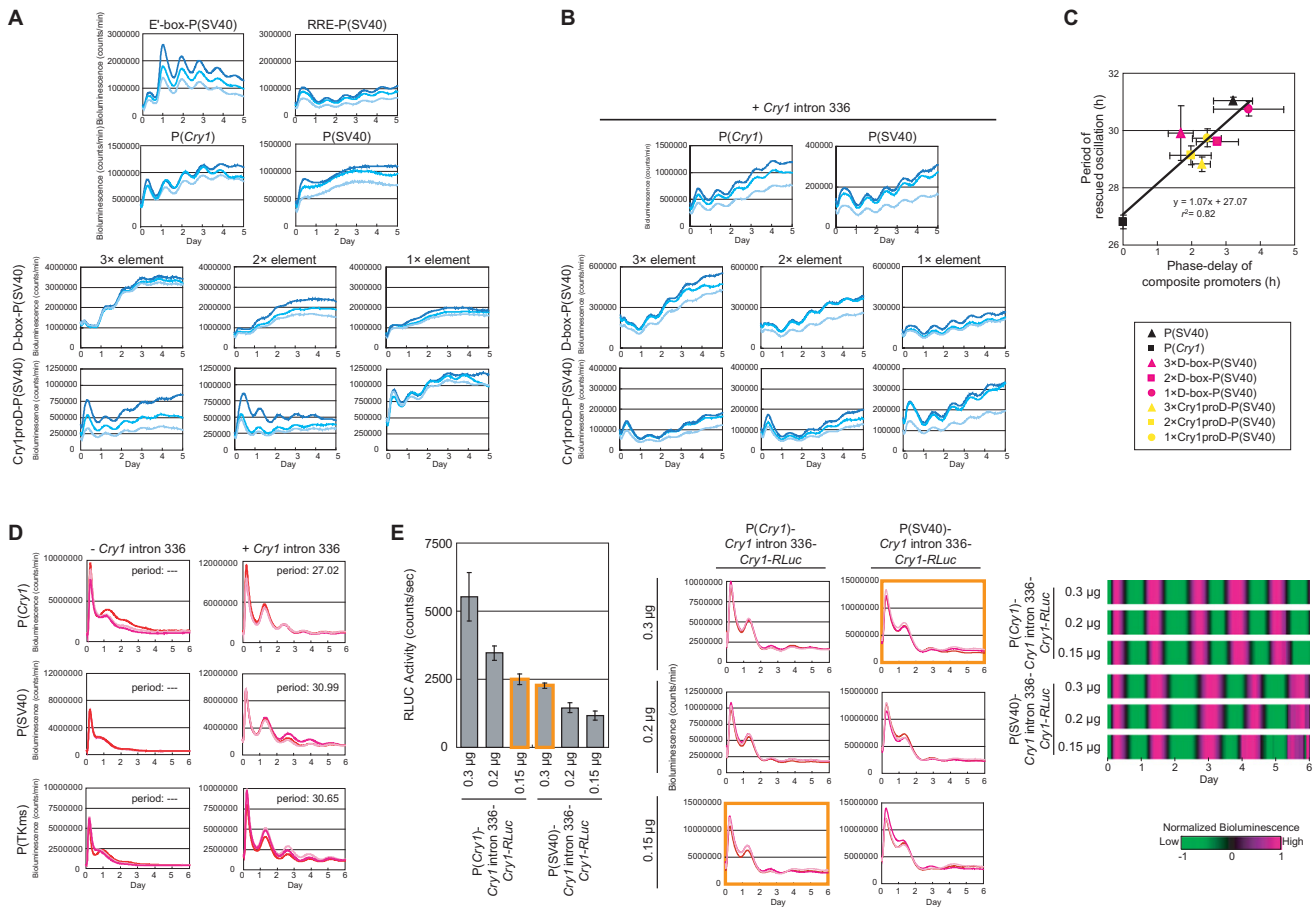
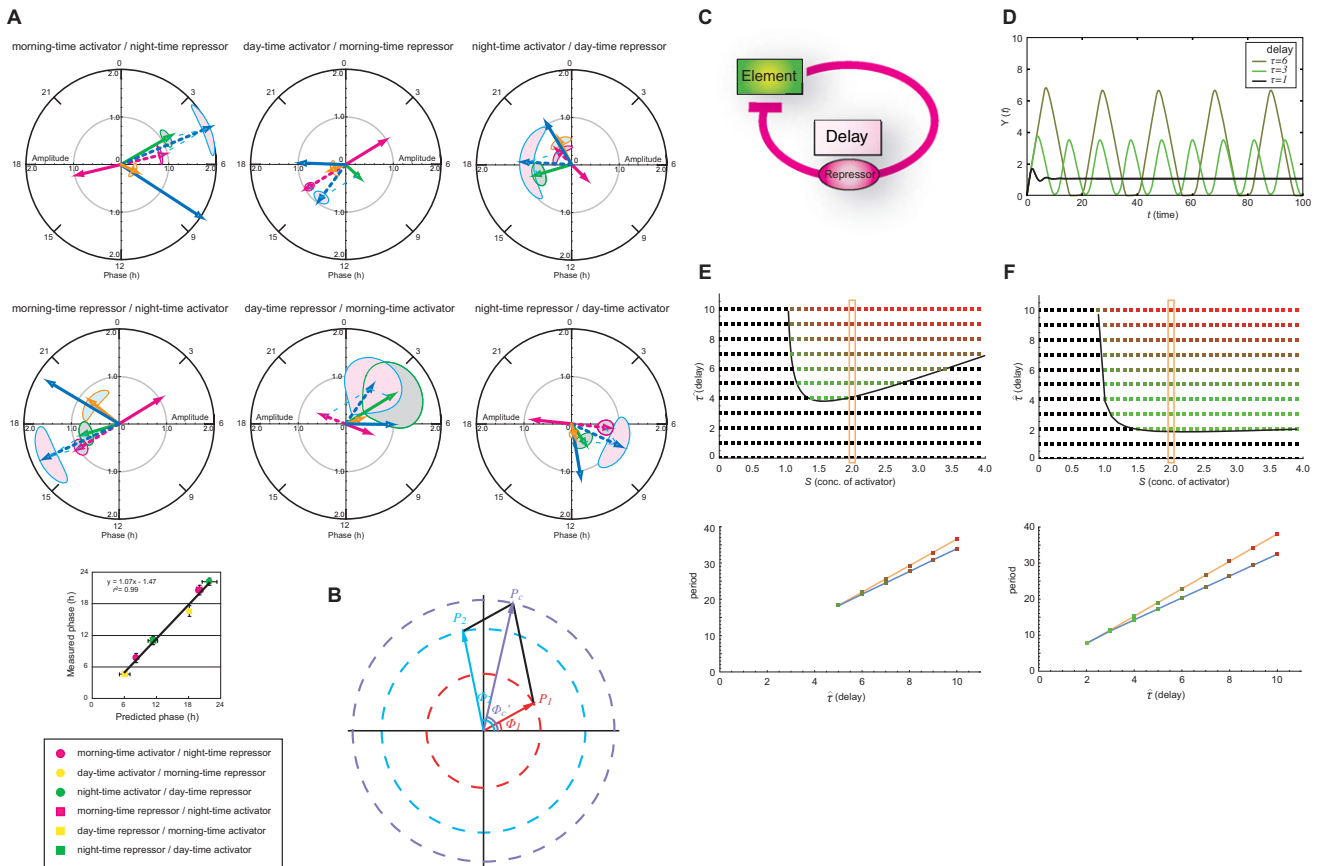**Figure S6. Related to Figure 6**

(A) Raw data of bioluminescence time-series corresponding to heatmaps in Figure 6A.

(B) Raw data of bioluminescence time-series corresponding to heatmaps in Figure 6B.

(C) Prolonged phase-delay of *Cry1* expression correlates with lengthened period length of rescued oscillations. The period lengths of rescued oscillations are plotted against the phase delay exhibited by various composite promoters relative to P(*Cry1*)-*Cry1* intron 336-*Luc* activity. Data here and in Figure 6E are similar and each represents an independent experiment.

(D) Circadian oscillations in *Cry1*$^{-/-}$:*Cry2*$^{-/-}$ cells rescued by *Cry1* driven by a TK minimal promoter P(TKms). *Cry1*$^{-/-}$:*Cry2*$^{-/-}$ cells were co-transfected with P(*Per2*)-d*Luc* reporter plasmid and *Cry1* cDNA driven by P(*Cry1*), P(SV40), or P(TKms) in the absence (left) or presence (right) of 336bp of *Cry1* intron sequence. P(*Per2*)-d*Luc* reporter activity in transfected *Cry1*$^{-/-}$:*Cry2*$^{-/-}$ cells was recorded. Period lengths are indicated in each panel.

(E) Circadian oscillations in *Cry1*$^{-/-}$:*Cry2*$^{-/-}$ cells rescued by *Cry1-Renilla luciferase* (*Rluc*) fusion gene. To confirm that CRY1 protein level was not responsible for the changes in rescued period, we employed CRY1-Rluc fusion protein and generated *Cry1* rescue constructs, in which *Cry1-Rluc* is driven by the combination of the wild-type *Cry1* intron sequence with either *Cry1* promoter or SV40 promoter. *Cry1*$^{-/-}$:*Cry2*$^{-/-}$ cells were transiently co-transfected with P(*Per2*)-d*Luc*, and various amounts (up to 2 fold) of *Cry1-Rluc* driven by P(*Cry1*) or P(SV40) with wild-type of 336bp of *Cry1* intron sequence. The RLUC activities of each sample were measured (left panel). The construct containing SV40 promoter exhibited circadian oscillations that are ~4 hr longer than the construct containing *Cry1* promoter, irrespective of the different DNA amounts and the resulting different CRY1 protein levels. Error bars represent SD (n = 3). P(*Per2*)-d*Luc* reporter activity in transfected *Cry1*$^{-/-}$:*Cry2*$^{-/-}$ cells expressing *Cry1-Rluc* was recorded (middle panels, n = 3). *Cry1-Rluc* expression was under the control of either P(*Cry1*) or P(SV40). The orange boxes indicate the similar amount of *Cry1-Rluc* expression. Heatmaps represent average promoter activities from three independent samples (right heatmaps). Raw data was detrended for baseline and amplitude, and then scaled into a range of −1 to 1. Data are representative of two independent experiments (A–E).

Figure S7. Phase Vector and Addition of Waves, Period of Negative Feedback Loop with Time Delay, Related to Figure 7 and Referenced in Extended Experimental Procedures

(A) A phase vector model recapitulates novel phases emerged from the combination of a transcriptional activator and a repressor. Plotted in the polar coordinate are phase vectors of transcriptional activators (green arrow) and repressors (solid red arrow) driven by morning-time (E' box), day-time (D box), or night-time (RRE) elements. The phase vector of the repressor is 180° rotated to represent its repression effect (dashed red arrow). Vector sum of activator- and repressor-vectors is represented by dashed blue arrow. Predicted phase vector is represented by solid blue arrow, which took into account the time-delay associated with transcription & translation of the regulator and *Luciferase* proteins (which was estimated in the previous report; ~4 hr (Ukai-Tadenuma et al., 2008)). Measured phase vectors emerged from combinatorial regulation (orange arrow) are consistent with predicted phase vectors (solid blue arrow), exhibiting significant correlation (bottom panel). See also Table S4. Error bars represent SD (n = 3).

(B) Phase vector and addition of waves. The component waves f_1 and f_2 are displayed as phase vectors P_1 and P_2. The length and direction of phase vectors represent phase and amplitude of corresponding waves. P_c is the summed phase vector of P_1 and P_2. See the sub-section 'Phase vector and addition of waves' in Extended Experimental Procedures.

(C–F) Period of negative feedback loop with time delay.

(C) A simple negative feedback loop with time delay is schematically illustrated. The expression of repressor is driven by a regulatory element, and the expressed repressor suppresses the element's activity with time delay.

(D) Numerical simulation of the model illustrated in (C). The period of oscillation increases as time delay (τ) increases. Under a critical value of time delay, oscillation dampens.

(E and F) Constraints on two variables ($\hat{\tau}$, S) for generating oscillation under certain values of synthesis and turnover rate ($k_1 = 1$ and $k_2 = 1$ respectively), the concentration of protease ($E_T = 1$), dissociation constant ($K_d = 1$) and Michaelis constant ($K_m = 0.1$). These graphs were drawn at two different Hill coefficients (p): p = 1 on (E), and p = 2 on (F). In the area of dimensionless time delay ($\hat{\tau}$) and the concentration of activator (S) above the curves, the model displays oscillation with period indicated by colored rectangles (green to red: short to long period, black: dampened or no sustained oscillation). The proportional relation of oscillation period with time delay ($\hat{\tau}$) is illustrated on bottom panels at the value of S = 2. The orange lines were calculated by the equation derived in the text (Equation (14, 15)). The blue lines were calculated by the numerical simulations. The period of numerical simulation was measured as difference of two neighboring peak times. (See also Extended Experimental Procedures.)